

Achieving wavenumber robustness in domain decomposition for heterogeneous Helmholtz equation: an overview of spectral coarse spaces

Victorita Dolean^{*,1}, Mark Fry^{†,2}, Matthias Langer^{‡,2}, Emile Parolin^{§,3}, and Pierre-Henri Tournier^{¶,3}

¹*Eindhoven University of Technology, PO Box 513, Eindhoven, 5600 MB, The Netherlands*

²*University of Strathclyde, 26 Richmond Street, Glasgow, G1 1XH, United Kingdom*

³*Sorbonne Université, Université Paris Cité, CNRS, INRIA, Laboratoire Jacques-Louis Lions, LJLL, EPC ALPINES, 4 place Jussieu, F-75005 Paris, France*

Abstract

Solving time-harmonic wave propagation problems in the frequency domain within heterogeneous media poses significant mathematical and computational challenges, particularly in the high-frequency regime. Among the available numerical approaches, domain decomposition methods are widely regarded as effective due to their suitability for parallel computing and their capacity to maintain robustness with respect to physical parameters, such as the wavenumber. These methods can achieve near-constant time-to-solution as the wavenumber increases, though often at the expense of a computationally intensive coarse correction step. This work focuses on identifying the best algorithms and numerical strategies for benchmark problems modelled by the Helmholtz equation. Specifically, we examine and compare several coarse spaces which are part of different families, e.g. GenEO (Generalised Eigenvalue Overlap) type coarse spaces and harmonic coarse spaces, that underpin two-level domain decomposition methods. By leveraging spectral information and multiscale approaches, we aim to provide a comprehensive overview of the strengths and weaknesses of these methods. Numerical experiments demonstrate that the effectiveness of these coarse spaces depends on the specific problem and numerical configuration, highlighting the trade-offs between computational cost, robustness, and practical applicability.

Keyword Helmholtz equation, domain decomposition method, two-level method, coarse space, high frequency

MSC codes 65N55, 65N35, 65F10

1 Introduction

The main focus of this work is tackling the computational complexity inherent in frequency-domain simulations of wave propagation and scattering for heterogeneous problems. These challenges are prevalent in various engineering fields, including acoustics, electromagnetic analysis, and seismic imaging. The finite element discretisation of frequency-domain wave models typically produces large-scale, indefinite, and poorly conditioned linear systems, which are especially difficult to handle with standard solvers. This difficulty escalates with high-frequency scenarios and intricate heterogeneities. Ensuring precision requires an increase in grid resolution at least proportional to frequency, making the resulting systems infeasible for direct solution methods in high-frequency cases. Consequently, the need arises for carefully tailored iterative techniques. This work focuses on two-level domain decomposition strategies aimed at efficiently solving these linear systems in parallel.

The wave behaviour is described by a heterogeneous Helmholtz equation posed on a computational domain $\Omega \subset \mathbb{R}^d$ ($d = 2, 3$), where the complex-valued field $u(\mathbf{x})$ satisfies

$$-\nabla \cdot (a(\mathbf{x}) \nabla u) - \omega^2 m(\mathbf{x}) u = f(\mathbf{x}) \quad \text{in } \Omega, \quad (1.1)$$

$$\mathcal{C}(u) = 0 \quad \text{on } \partial\Omega, \quad (1.2)$$

with \mathcal{C} representing the imposed boundary conditions, $a(\mathbf{x}) > 0$ a spatially varying coefficient associated with material stiffness (or inverse density), $m(\mathbf{x}) > 0$ a spatially varying “mass” coefficient related to the squared slowness, $\omega > 0$ the angular frequency, $c(\mathbf{x})$ the wave speed and $f(\mathbf{x})$ the source term.

^{*}v.dolean.maini@tue.nl

[†]mark.fry@strath.ac.uk

[‡]m.langer@strath.ac.uk

[§]emile.parolin@inria.fr

[¶]pierre-henri.tournier@sorbonne-universite.fr

The local wavenumber is given by

$$k(\mathbf{x}) = \omega \sqrt{\frac{m(\mathbf{x})}{a(\mathbf{x})}},$$

which reduces to the familiar relation $k(\mathbf{x}) = \omega/c(\mathbf{x})$ when $a \equiv 1$ and $m(\mathbf{x}) = c^{-2}(\mathbf{x})$. In heterogeneous media, spatial variations in a and m lead to additional variations in $k(\mathbf{x})$, making the high-frequency regime (large k) particularly challenging for numerical solvers.

The challenges of developing effective solvers for the Helmholtz equation are well documented in reviews such as [21, 27], which highlight the difficulty in extending state-of-the-art methods for symmetric positive definite problems to handle the indefinite or non-self-adjoint nature of the Helmholtz problem. For large-scale problems—where accurate discretisation for high wavenumbers is required—domain decomposition methods emerge as a natural approach [18]. Despite recent advances, both theoretical [33, 34, 30] and numerical [15, 19, 47, 45], we are still at the stage where *no single method has consistently outperformed others in addressing the solution of the discretised Helmholtz equation in high frequency regime*.

Domain decomposition methods are widely used for solving large systems arising from PDE discretisation, offering robust strategies for various problems. However, traditional methods often fail or even diverge when applied to wave propagation problems. One critical aspect requires careful attention: the coarse space that captures global behaviour and facilitates distant inter-domain information transfer while dealing with the non-locality of the wave phenomena. This work focuses on overlapping Schwarz methods which are robust against the physical coefficients (wavenumber and heterogeneity) of the problem and scalable as the number of subdomains increases. Addressing these challenges requires coarse information that is both computationally efficient and globally accessible to all subdomains. This study emphasises once again the importance of sophisticated coarse spaces specially tailored to the nature of the problem.

One of the prominent methods to tackle complex problems with large contrasts in the physical coefficients is the GenEO (Generalised Eigenproblems in the Overlap) coarse space which has proven effective for solving highly heterogeneous elliptic problems [46, 35]. However, for the Helmholtz equation, selecting an appropriate coarse space is particularly challenging. Due to its indefinite or non-self-adjoint nature, enlarging the coarse space does not necessarily enhance performance [24]. Designing coarse spaces for the Helmholtz problem also involves minimising dependence on the wavenumber k . Using plane waves as a coarse space basis is a natural approach for capturing global behaviour, but their suitability for heterogeneous media remains uncertain. Plane waves were first applied in multigrid methods [12] and later extended to domain decomposition methods, such as FETI-(DP)-H [23, 22], though primarily for homogeneous problems.

Even though coarse space information must be globally available, coarse spaces can be constructed locally using basis vectors derived from solutions to local eigenvalue problems. Spectral coarse spaces, such as the DtN (Dirichlet-to-Neumann) coarse space, illustrate this approach for the Helmholtz equation [14]. These eigenproblems are formulated on subdomain interfaces using a DtN map, building on methods developed for elliptic problems [44, 20]. Due to the difficulty in obtaining theoretical results for these kinds of problems, the first assessment of two different yet related spectral coarse spaces—the DtN method and a GenEO-type approach tailored to the Helmholtz problem—was done in [8] for simple test cases. At the same time in [11] the authors have synthesised recent advancements in enhancing domain decomposition methods for heterogeneous media and implemented these approaches using a common software framework, FreeFEM. Practical implementation details and trade-offs were thoroughly discussed there, and extensive numerical experiments on 2D and 3D benchmark problems were presented to evaluate and compare the methods in various settings. Finally, those results provide guidance on the suitability of different methods for specific scenarios, offering insights for future applications.

More recently, a new family of coarse spaces has emerged, inspired by the multiscale spectral generalised finite element method (MS-GFEM). In [42] the authors introduce global coarse solves derived from MS-GFEM spaces constructed through local eigenproblems and prove that the preconditioner, when used with GMRES, achieves convergence at a rate tied to the MS-GFEM approximation error, and since MS-GFEM exhibits exponential convergence due to oversampling this will ensure efficient performance with a small coarse space. This work provides a robust and scalable strategy for solving heterogeneous Helmholtz problems, particularly in high-frequency regimes. Akin to this philosophy [38] relies on coarse spaces based on generalised eigenvalue problems on harmonic spaces composed of Helmholtz extensions. Besides, [26] provides a general theoretical framework of two-level methods for Helmholtz. Another approach has been described in [43], and provides a systematic way of constructing coarse spaces for possibly non-Hermitian and indefinite matrices hence applicable to the linear systems arising from the discretisation of the Helmholtz equation. Finally, we mention [1] which provides a fully algebraic coarse space construction that has been applied to indefinite or non-symmetric matrices, with available analysis only for SPD matrices.

Although the previous methods are theoretically sound, they may face several limitations that may impact their practical applicability. The convergence theory relies on assumptions, which may not hold in real-world scenarios. While methods are introduced in a general setting, their scalability for large-scale 3D problems and heterogeneous media remains unproven. Additionally, the practical utility of coarse spaces, including both problem-adapted and non-adapted basis functions, is uncertain, as the results may not translate into computationally efficient

implementations. The focus on theoretical rigor over implementation leaves challenges like the cost of coarse space construction and computational bottlenecks unaddressed. Furthermore, the preconditioner’s performance may still be heavily influenced by problem-specific parameters, raising concerns about robustness in practical settings.

Our main contributions are:

- We provide the first unified and reproducible comparison of all major spectral coarse space families for the heterogeneous, high-frequency Helmholtz equation—implemented within a common FreeFEM framework.
- We carry out large-scale numerical experiments on both simple test cases and challenging 2D/3D benchmarks, revealing new insights into robustness, scalability, and computational cost.
- We provide practical guidance on when and how each coarse space is most effective, offering actionable recommendations for real-world Helmholtz solvers.

Building on the earlier comparative study of coarse spaces for the Helmholtz equation in the high-frequency regime [11], this work substantially extends the scope and depth of the analysis. In particular, we incorporate the most recent advances in coarse space design—most notably the emerging family of Helmholtz-harmonic and extended harmonic coarse spaces—and examine them alongside established DtN and GenEO-type approaches. The numerical evaluation goes far beyond previous work: we explore performance across a wide spectrum of 2D and 3D benchmark problems, from idealised homogeneous cases to challenging heterogeneous, high-contrast, and realistic large-scale geometries, pushing the limits of current two-level methods. This leads to new insights into the trade-offs between robustness, coarse space size, and computational cost, and clarifies the conditions under which each approach is most effective.

The paper is organised as follows. Section 2 introduces the heterogeneous Helmholtz problem, its boundary value formulation, and finite element discretisation. Section 3 outlines the foundations of domain decomposition methods and motivates the introduction of a second-level (coarse space) correction via deflation. Section 4 presents the three main families of coarse spaces—DtN, GenEO-type, and harmonic—together with their recent variants. Section 5 provides an extensive set of numerical experiments, covering both controlled test cases and realistic large-scale applications. Conclusions and perspectives are discussed in Section 6.

2 Discretisation of the heterogeneous Helmholtz problem

We focus here on the interior heterogeneous Helmholtz problem (1.1) with suitable boundary conditions. In practical settings, the domain is truncated to a bounded computational domain Ω , and the far-field Sommerfeld radiation condition must be approximated on the artificial boundary of Ω to model wave behaviour appropriately. A widely used approximation is the Robin (impedance) condition, though alternatives include absorbing boundary conditions (ABCs) [49] or perfectly matched layers (PML) [36, 4]. We consider Dirichlet conditions on $\Gamma_D \subset \partial\Omega$ and Robin conditions on $\Gamma_R = \partial\Omega \setminus \Gamma_D$, solving the boundary value problem:

$$-\nabla \cdot (a(\mathbf{x}) \nabla u) - \omega^2 m(\mathbf{x}) u = f(\mathbf{x}) \quad \text{in } \Omega, \quad (2.1a)$$

$$u = u_{\Gamma_D} \quad \text{on } \Gamma_D, \quad (2.1b)$$

$$a(\mathbf{x}) \frac{\partial u}{\partial \mathbf{n}} + i \omega Z(\mathbf{x}) u = 0 \quad \text{on } \Gamma_R, \quad (2.1c)$$

where \mathbf{n} is the outward normal, and $Z(\mathbf{x})$ is an impedance coefficient typically chosen as $Z(\mathbf{x}) = \sqrt{a(\mathbf{x}) m(\mathbf{x})}$ to approximate the Sommerfeld radiation condition. The problem is well posed if $\Gamma_R \neq \emptyset$ but may become ill-posed for certain parameter choices when $\Gamma_R = \emptyset$. The local wavenumber $k(\mathbf{x})$ can vary within Ω and may have discontinuities across material interfaces, allowing $k \in L^\infty(\Omega)$.

For $\Omega' \subset \Omega$, the trial and test spaces are defined as

$$V(\Omega') = \{u \in H^1(\Omega') : u = u_{\Gamma_D} \text{ on } \Gamma_D \cap \partial\Omega'\}, \quad V_0(\Omega') = \{u \in H^1(\Omega') : u = 0 \text{ on } \Gamma_D \cap \partial\Omega'\}. \quad (2.2)$$

The weak formulation seeks $u \in V(\Omega)$ satisfying:

$$a_\Omega(u, v) = F(v), \quad \forall v \in V_0(\Omega), \quad (2.3)$$

where, for any $\Omega' \subset \Omega$, we define:

$$a_{\Omega'}(u, v) = \int_{\Omega'} (a(\mathbf{x}) \nabla u \cdot \nabla \bar{v} - \omega^2 m(\mathbf{x}) u \bar{v}) \, d\mathbf{x} + \int_{\Gamma_R \cap \partial\Omega'} i \omega Z(\mathbf{x}) u \bar{v} \, ds, \quad F(v) = \int_{\Omega} f \bar{v} \, d\mathbf{x}. \quad (2.4)$$

Using a simplicial mesh \mathcal{T}^h of Ω with element diameter h , we use finite elements to discretise (2.3), as outlined in [11]. A Lagrange finite element approximation reduces the problem to solving the complex linear system:

$$\mathbf{A} \mathbf{u} = \mathbf{f}, \quad (2.5)$$

where $A \in \mathbb{C}^{n \times n}$ and $\mathbf{f} \in \mathbb{C}^n$ are respectively derived from the sesquilinear and antilinear forms, and n denotes the total number of degrees of freedom in Ω . Accurate approximation requires fine discretisation, particularly as $k(\mathbf{x})$ increases, due to the pollution effect [3]. For piecewise linear (\mathbb{P}_1) elements, maintaining accuracy requires $k_{\max}^3 h^2$ to remain bounded, where $k_{\max} = \sup_{\mathbf{x} \in \Omega} k(\mathbf{x})$, implying $h = \mathcal{O}(k_{\max}^{-3/2})$. Higher-order elements relax this constraint, but interpolation properties degrade for very high orders. An alternative common strategy is to fix the number of points per wavelength, n_{ppwl} , with $h = \mathcal{O}(k_{\max}^{-1})$, where the wavelength is $\lambda(\mathbf{x}) = 2\pi/k(\mathbf{x})$. Practitioners often use 5 or 10 points per wavelength.

3 Domain decomposition methods

To solve the discrete heterogeneous Helmholtz problem (2.5), we employ GMRES with acceleration provided by a two-level overlapping domain decomposition preconditioner. The core one-level approach used is the optimised restricted additive Schwarz (ORAS) method [18]. To formulate the domain decomposition preconditioner, we begin by dividing the domain Ω into a set of N non-overlapping subdomains $\{\Omega'_s\}_{s=1}^N$, which align with the finite element mesh \mathcal{T}^h . Overlapping subdomains $\{\Omega_s\}_{s=1}^N$ are then created by expanding each Ω'_s with neighbouring mesh elements, defined as:

$$\Omega_s = \text{Int} \left(\bigcup_{\text{supp}(\phi_j) \cap \Omega'_s \neq \emptyset} \text{supp}(\phi_j) \right),$$

where $\text{Int}(\cdot)$ and $\text{supp}(\cdot)$ represent the interior and support of a function, respectively, and ϕ_j are the nodal basis functions of the finite element space. Additional layers can be recursively added to increase the overlap as needed.

With the overlapping decomposition, we define the preconditioner components. The restriction operator $R_s \in \mathbb{R}^{n_s \times n}$ restricts functions to Ω_s where n_s denotes the local number of degrees of freedom in Ω_s , while the transpose R_s^T extends by zero outside Ω_s . A partition of unity is represented by diagonal matrices $D_s \in \mathbb{R}^{n_s \times n_s}$, ensuring

$$\sum_{s=1}^N R_s^T D_s R_s = I.$$

ORAS also requires solving local heterogeneous Helmholtz–Robin problems:

$$-\nabla \cdot (a(\mathbf{x}) \nabla w_s) - \omega^2 m(\mathbf{x}) w_s = f \quad \text{in } \Omega_s, \quad (3.1a)$$

$$a(\mathbf{x}) \frac{\partial w_s}{\partial \mathbf{n}_s} + i \omega Z(\mathbf{x}) w_s = 0 \quad \text{on } \partial\Omega_s \setminus \partial\Omega, \quad (3.1b)$$

$$\mathcal{C}(w_s) = 0 \quad \text{on } \partial\Omega_s \cap \partial\Omega, \quad (3.1c)$$

where \mathcal{C} applies the boundary conditions (2.1b)–(2.1c), and $Z(\mathbf{x})$ is the local impedance, typically chosen as $Z(\mathbf{x}) = \sqrt{a(\mathbf{x})m(\mathbf{x})}$. The finite element discretisation of (3.1) yields a local stiffness matrix $\hat{A}_s \in \mathbb{C}^{n_s \times n_s}$. The ORAS preconditioner is then assembled as:

$$M_{\text{ORAS}}^{-1} = \sum_{s=1}^N R_s^T D_s \hat{A}_s^{-1} R_s,$$

where the local solves \hat{A}_s^{-1} are performed in parallel.

To ensure robustness and scalability, particularly for indefinite problems like the Helmholtz equation, the ORAS method incorporates a coarse space in a two-level framework. The coarse space, represented by a matrix Z with linearly independent column vectors, plays a key role in addressing scalability. Using deflation, a coarse operator $E = Z^\dagger A Z$ and correction operator $Q = Z E^{-1} Z^\dagger$ are defined, yielding the two-level ORAS method:

$$M_{\text{ORAS},2}^{-1} = M_{\text{ORAS}}^{-1} (I - A Q) + Q.$$

The choice of coarse space is critical, particularly for indefinite problems where its addition may not always improve performance [24]. We next discuss the selection of coarse spaces.

4 Spectral coarse spaces

In this study, we investigate spectral coarse spaces for the discrete Helmholtz problem (2.5), which are constructed by solving local eigenvalue problems on subdomains and assembling the resulting eigenfunctions into a global coarse space. While a broad family of such spectral coarse spaces exists, we focus on two representative classes that follow a similar construction philosophy: **GenEO-type spaces** and **harmonic-type spaces**.

We begin by reviewing the DtN coarse space introduced in [14], then present the Δ -GenEO [9, 16] and H_k -GenEO spaces [13], which are inspired by the GenEO methodology [46]. In parallel, we consider recently developed Helmholtz-harmonic coarse spaces from [38, 42, 43]. Finally, we establish connections between these approaches.

Although comparative analyses were conducted in [11, 8], our study builds upon and extends them by incorporating the latest developments in the field, along with a detailed complexity analysis on both model and benchmark problems. Note that in light of the same recent developments the DtN coarse space can be both considered as an ancestor of GenEO coarse spaces but also, by construction, falls into the category of harmonic coarse spaces.

Notation: Given a variational problem with system matrix B , we denote by B_s the local Dirichlet matrix on subdomain Ω_s . If Robin boundary conditions are imposed on internal interfaces, the corresponding local matrix is denoted by \tilde{B}_s , whereas for Neumann boundary conditions we write \tilde{B}_s .

4.1 The DtN Coarse space

We begin by revisiting the Dirichlet-to-Neumann (DtN) coarse space, originally introduced in [44] for elliptic problems and extended to the Helmholtz equation in [14]. This method constructs the coarse space from the low-frequency eigenmodes of a boundary operator defined via local DtN maps, which are then extended harmonically inside each subdomain. From a broader perspective, the DtN approach can be viewed as an early instance of harmonic-type coarse spaces, and also as a precursor to GenEO-type constructions that build on similar principles of localised spectral analysis.

Let $\Gamma_s = \partial\Omega_s \setminus \partial\Omega$ denote the interface between subdomain Ω_s and its neighbours. Given Dirichlet data v_{Γ_s} on Γ_s , the local heterogeneous Helmholtz extension is the solution v of the boundary value problem:

$$-\nabla \cdot (a(\mathbf{x})\nabla v) - \omega^2 m(\mathbf{x})v = 0 \quad \text{in } \Omega_s, \quad (4.1a)$$

$$v = v_{\Gamma_s} \quad \text{on } \Gamma_s, \quad (4.1b)$$

$$\mathcal{C}(v) = 0 \quad \text{on } \partial\Omega_s \cap \partial\Omega, \quad (4.1c)$$

where $\mathcal{C}(v) = 0$ enforces the original problem boundary conditions. The DtN map then takes v_{Γ_s} to its corresponding Neumann data on Γ_s :

$$\text{DtN}_{\Omega_s}(v_{\Gamma_s}) = a(\mathbf{x}) \frac{\partial v}{\partial n} \Big|_{\Gamma_s}. \quad (4.2)$$

The DtN eigenproblem for subdomain Ω_s is

$$\text{DtN}_{\Omega_s}(u_{\Gamma_s}) = \lambda u_{\Gamma_s}, \quad (4.3)$$

where u_{Γ_s} are eigenfunctions with eigenvalues $\lambda \in \mathbb{C}$. The corresponding coarse space is constructed by taking the heterogeneous Helmholtz extension of u_{Γ_s} in Ω_s and extending it by zero across Ω via the partition of unity [14].

For the discrete setting, we introduce local Neumann matrices \tilde{A}_s , where $\mathcal{C} = 0$ on $\partial\Omega_s \cap \partial\Omega$. Let Γ_s and I_s denote boundary and interior indices, respectively. Defining the mass matrix on the interface as $M_{\Gamma_s} = \left(\int_{\Gamma_s} \phi_j \phi_i \right)_{i,j \in \Gamma_s}$ the discrete DtN eigenproblem is given by

$$\left(\tilde{A}_{\Gamma_s, \Gamma_s} - A_{\Gamma_s, I_s} A_{I_s, I_s}^{-1} A_{I_s, \Gamma_s} \right) \mathbf{u}_{\Gamma_s} = \lambda M_{\Gamma_s} \mathbf{u}_{\Gamma_s}, \quad (4.4)$$

where A_{I_s, Γ_s} , A_{Γ_s, I_s} and A_{I_s, I_s} , A_{Γ_s, Γ_s} are obvious notations for sub-blocks of matrix A corresponding to the set of indices in the interior I_s and on the boundary Γ_s . Because of the Robin boundary condition on Γ_R , the left-hand-side matrix in (4.4) is a priori non-Hermitian. The Helmholtz extension to interior degrees of freedom is obtained via $\mathbf{u}_{I_s} = -A_{I_s, I_s}^{-1} A_{I_s, \Gamma_s} \mathbf{u}_{\Gamma_s}$, and the global coarse basis in Z is formed as $R_s^T D_s \mathbf{u}_s$, where \mathbf{u}_s is the full local vector computed from \mathbf{u}_{Γ_s} and \mathbf{u}_{I_s} [14]. We see that the discrete counterpart of Equation (4.3) is Equation (4.4) consisting in a Schur complement based generalised eigenvalue problem.

A key aspect is the selection of eigenvectors for the coarse space. In [14] a criterion has been identified empirically consisting in retaining the eigenvalues with the smallest real parts, imposing the threshold

$$\text{Re}(\lambda) < \eta_{\max}. \quad (4.5)$$

While $\eta_{\max} = k_s$, where $k_s := \sup_{\mathbf{x} \in \Omega_s} k(\mathbf{x})$, was initially proposed, recent work [7, 8] suggests that $\eta_{\max} = k_s^{4/3}$ can improve robustness with respect to the wavenumber. Also in [8] this threshold was systematically studied and empirical k -dependent bounds were derived for the sizes of the corresponding coarse spaces.

Remark 4.1. Unlike for Laplace's equation with self-adjoint boundary conditions where generalised eigenvalue problems are self-adjoint and positive definite, the DtN eigenproblems for Helmholtz are in general non-self-adjoint. As a consequence, there are currently no theoretical convergence guarantees for the DtN coarse space. Nevertheless, recent studies—including [11] and [8]—demonstrate that this approach performs remarkably well in practice, and its complexity can be quantified empirically. A significant advantage of this construction is that its coarse space dimension is inherently limited by the number of degrees of freedom on the subdomain interface Γ_s , as the eigenfunctions are defined on Γ_s and only extended into the interior. This allows for global modes with full support to be generated from a relatively compact spectral basis.

4.2 GenEO-type coarse spaces: Δ -GenEO and H -GenEO

The Generalised Eigenproblems in the Overlap (GenEO) coarse space, introduced in [46], offers a robust approach for symmetric positive definite problems, even in heterogeneous settings. Note that originally, GenEO was formulated variationally under the assumption that the bilinear form $a_\Omega(\cdot, \cdot)$ is symmetric and coercive, assumption not satisfied here. Given a subdomain Ω_s and its overlapping region Ω_s° , the local eigenproblem is defined as

$$a_{\Omega_s}(u, v) = \lambda a_{\Omega_s^\circ}(\Xi_s(u), \Xi_s(v)) \quad \forall v \in V(\Omega_s), \quad (4.6)$$

where Ξ_s is the partition of unity operator. Here, $a_D(\cdot, \cdot)$ represents the variational problem restricted to domain D with problem boundary conditions on $\partial\Omega$ and natural conditions on $\partial D \setminus \partial\Omega$. The smallest eigenvalue λ not included in the GenEO space determines the preconditioned operator's condition number, making thresholding on $\lambda < \lambda_{\max}$ a natural choice. Alternatively, a fixed number of eigenvectors per subdomain can be selected for efficiency. The restriction to Ω_s° is not necessary, and a more practical variant replaces it with Ω_s , simplifying implementation [18]. This leads to the discrete eigenproblem

$$\tilde{A}_s \mathbf{u} = \lambda D_s A_s D_s \mathbf{u}, \quad (4.7)$$

where $A_s = R_s A R_s^T$ is the local Dirichlet matrix. The coarse space basis in Z is then constructed as $R_s^T D_s \mathbf{u}$. This formulation will serve as the foundation for a Helmholtz-specific extension.

4.2.1 Δ -GenEO coarse space

Applying GenEO to the Helmholtz problem is challenging due to the loss of self-adjointness and definiteness. While theoretical advancements have been made [9, 10], a fully justified spectral coarse space for Helmholtz remains elusive. One workaround, Δ -GenEO, replaces the Helmholtz operator with the Laplacian (setting $\omega = 0$ in Equation (2.1) and Equation (2.4)), yielding the eigenproblem

$$\tilde{L}_s \mathbf{u} = \lambda D_s L_s D_s \mathbf{u}, \quad (4.8)$$

where L_s and \tilde{L}_s are the local Laplace Dirichlet and Neumann matrices, respectively. This provides a well-posed problem with real non-negative eigenvalues, but its effectiveness deteriorates as k increases since Laplace solutions diverge significantly from those of Helmholtz. For this coarse space theoretical bounds have been rigorously established in [9] and further improved in [16]. These bounds show, as expected, that this coarse space cannot perform very effectively at high frequencies and the size of the coarse space increases dramatically with the frequency.

4.2.2 The H_k -GenEO coarse space

To construct a more suitable spectral coarse space for the heterogeneous Helmholtz problem, it is essential to incorporate the Helmholtz operator itself. However, directly applying Equation (4.7) with the heterogeneous operator leads to a non-self-adjoint problem with complex eigenvalues, which can cause solver instability. Instead, we propose a hybrid approach that links the indefinite heterogeneous Helmholtz operator to a positive-definite surrogate operator. The local eigenproblem is given by

$$\tilde{A}_s \mathbf{u} = \lambda D_s P_s D_s \mathbf{u}, \quad (4.9)$$

where:

- \tilde{A}_s is the local Neumann matrix for the heterogeneous Helmholtz operator

$$-\nabla \cdot (a(\mathbf{x}) \nabla u) - \omega^2 m(\mathbf{x}) u,$$

- D_s is the local partition-of-unity weighting matrix,
- P_s is a symmetric positive-definite (SPD) matrix chosen to be “close” to A_s in a suitable sense.

A natural choice for P_s is L_s , the discretisation of the Laplace operator $-\Delta$ with heterogeneous coefficient $a(\mathbf{x})$. In practice, many SPD choices perform well, but another particularly convenient choice—allowing for simpler theoretical estimates—is $P_s = B_s$, where B_s is the discretisation of the *positive* heterogeneous Helmholtz operator

$$-\nabla \cdot (a(\mathbf{x}) \nabla u) + \omega^2 m(\mathbf{x}) u. \quad (4.10)$$

The corresponding method is called H_k -GenEO, and theoretical estimates have been derived for the indefinite heterogeneous Helmholtz problem in [13]. When Robin conditions are used, the eigenvalues of (4.9) are complex but tend to cluster near the real axis, enabling a stable selection criterion based on

$$\text{Re}(\lambda) < \eta_{\max}.$$

A thorough numerical study performed in [8] shows that H_k -GenEO achieves wavenumber-independent GMRES convergence and empirical frequency scaling formulae were derived. A robust and commonly used choice is $\eta_{\max} = \frac{1}{2}$.

Remark 4.2. Unlike the DtN coarse space, where the spectral information is extracted from the subdomain boundary and then harmonically extended into the interior, the GenEO family constructs eigenproblems that are defined throughout each subdomain, often including the overlap region. This leads to potentially larger coarse spaces since the spectral basis is built over the full subdomain volume.

Although a full theoretical analysis of the GenEO methodology in the Helmholtz context is still incomplete, rigorous convergence estimates are available for certain variants. In particular, for Δ -GenEO, such bounds were established in [9] and later refined in [16]. These results were recently extended to the H_k -GenEO construction [13]. However, these theoretical results tend to be conservative, often overestimating the coarse space size required in practice. Numerical experiments indicate that both GenEO variants exhibit significantly better performance than what the theory predicts.

4.3 Helmholtz-harmonic coarse spaces

We now describe the class of *Helmholtz-harmonic coarse spaces*, introduced independently in [42, 38] and later in a fully algebraic setting in [43]. These spaces are built from discrete solutions of the *heterogeneous* Helmholtz equation on local subdomains and then assembled into a global conforming approximation space using partition-of-unity weights.

4.3.1 Harmonic GenEO coarse space

The underlying philosophy is similar in spirit to the *GenEO family*: a local spectral decomposition is used to select relevant low-energy modes that define the coarse space. However, there is a key distinction: while GenEO formulates a spectral problem using the full operator (e.g. Laplacian or Helmholtz) and searches for dominant directions in the whole local space, *harmonic coarse spaces restrict the search space to local Helmholtz-harmonic functions*. The spectral problem is then posed over this smaller subspace typically associated with the *positive* heterogeneous Helmholtz operator (4.10). This restriction makes the underlying spectral theory easier and the coarse space selection process *real-valued*, while still encoding the Helmholtz physics through the choice of constrained subspace.

To introduce the coarse spaces described in [42, 38], we begin by defining the *space of local Helmholtz solutions* on a subdomain Ω_s :

$$W(\Omega_s) := \{u \in V(\Omega_s) : a_{\Omega_s}(u, v) = 0, \forall v \in V_0(\Omega_s)\}, \quad (4.11)$$

where $V(\Omega_s)$ and $V_0(\Omega_s)$ are defined in (2.2). The sesquilinear form $a_{\Omega_s}(\cdot, \cdot)$ corresponds to the Helmholtz operator defined in (2.4). Thus, $W(\Omega_s)$ consists of heterogeneous Helmholtz solutions with the appropriate boundary conditions.

To define a spectral selection on this space, we introduce the *positive heterogeneous Helmholtz sesquilinear form*:

$$b_{\Omega_s}(u, v) = \int_{\Omega_s} (a(\mathbf{x}) \nabla u \cdot \nabla \bar{v} + \omega^2 m(\mathbf{x}) u \bar{v}) \, d\mathbf{x}. \quad (4.12)$$

We then solve the following eigenproblem (see [38, eq. (3.6)] and [42, eq. (2.20)]):

$$\text{find } u \in W(\Omega_s) \text{ such that } b_{\Omega_s}(u, v) = \lambda b_{\Omega_s}(\Xi_s(u), \Xi_s(v)) \quad \forall v \in W(\Omega_s), \quad (4.13)$$

where Ξ_s is the partition-of-unity operator associated with the subdomain Ω_s . This problem is *self-adjoint and coercive*, and all eigenvalues λ are real and positive.

To handle the Helmholtz-harmonicity constraint in practice, the eigenvalue problem is recast as a saddle point problem [42, eq. (2.27)]: find $u \in V(\Omega_s)$, $p \in V_0(\Omega_s)$, $p = 0$ on $\partial\Omega_s \setminus \partial\Omega$ such that

$$b_{\Omega_s}(u, v) + \overline{a_{\Omega_s}(v, p)} = \lambda b_{\Omega_s}(\Xi_s(u), \Xi_s(v)), \quad \forall v \in V(\Omega_s), \quad (4.14)$$

$$a_{\Omega_s}(u, q) = 0, \quad \forall q \in V_0(\Omega_s), \quad (4.15)$$

$$p = 0, \quad \text{on } \partial\Omega_s \setminus \partial\Omega. \quad (4.16)$$

In matrix notations, the eigenproblem system is: find \mathbf{u} and \mathbf{p} such that

$$\begin{bmatrix} \tilde{B}_s & A_{s,0}^* \\ A_{s,0} & 0 \end{bmatrix} \begin{bmatrix} \mathbf{u} \\ \mathbf{p} \end{bmatrix} = \lambda \begin{bmatrix} D_s B_s D_s & 0 \\ 0 & 0 \end{bmatrix} \begin{bmatrix} \mathbf{u} \\ \mathbf{p} \end{bmatrix}, \quad (4.17)$$

where:

- $A_s = R_s A R_s^T$ is the local Dirichlet matrix associated with the heterogeneous Helmholtz sesquilinear form a_{Ω_s} ,
- $A_{s,0}$ is the restriction of A_s to rows not associated with boundary nodes,
- $B_s = R_s B R_s^T$ is the local Dirichlet matrix associated with the positive Helmholtz bilinear form b_{Ω_s} ,

- \tilde{B}_s is its Neumann counterpart,
- D_s is the partition of unity diagonal weight matrix.

For simplicity, the system above was written for homogeneous Dirichlet boundary conditions $u_{\Gamma_D} = 0$.

After solving the eigenproblem, the *coarse space basis* is formed by selecting all eigenvectors \mathbf{u} associated with eigenvalues $\lambda < \tau$, where $\tau > 0$ is a user-defined threshold. These are then extended to the global space via:

$$Z = \{R_s^T D_s \mathbf{u}\}.$$

Each basis function is thus globally supported (via the partition of unity), locally Helmholtz-harmonic (by construction), and selected through a stable positive definite spectral problem.

4.3.2 Extended Harmonic GenEO coarse space

Building on the construction of Helmholtz-harmonic coarse spaces described above, we now present a fully algebraic variant introduced in [43]. This approach retains the same core philosophy—constructing coarse functions from locally Helmholtz-harmonic components—but introduces an *extended overlapping decomposition*. Contrary to the previous variant, the discrete Helmholtz-harmonic constraint is not enforced on the eigenvectors, but rather in the construction of the coarse space matrix Z thanks to a suitable operator (also present in the eigenproblem).

Specifically, for each original subdomain Ω_s , an enlarged subdomain $\tilde{\Omega}_s$ is defined by adding at least one layer of mesh elements along its interfaces with neighbouring subdomains. This auxiliary decomposition $\{\tilde{\Omega}_s\}_{s=1}^N$ is used solely for the construction of the coarse space and does *not* affect the first-level (fine-scale) preconditioner.

All quantities associated with the extended subdomains are denoted with a superscript \checkmark . For example, \check{R}_s is the restriction matrix to $\tilde{\Omega}_s$, and $\check{A}_s = \check{R}_s A \check{R}_s^T$ is the local Dirichlet matrix on $\tilde{\Omega}_s$.

The local eigenproblem reads: find $\check{\mathbf{u}}$ such that

$$\tilde{B}_s \check{\mathbf{u}} = \lambda \left(R_s \check{R}_s^T - \hat{A}_s^{-1} R_s \check{R}_s^T \check{A}_s \right)^\dagger D_s B_s D_s \left(R_s \check{R}_s^T - \hat{A}_s^{-1} R_s \check{R}_s^T \check{A}_s \right) \check{\mathbf{u}}, \quad (4.18)$$

where:

- $\check{A}_s = \check{R}_s A \check{R}_s^T$ is the local Dirichlet matrix associated with the heterogeneous Helmholtz sesquilinear form $a_{\tilde{\Omega}_s}$ on the enlarged subdomain $\tilde{\Omega}_s$,
- $B_s = R_s B R_s^T$ is the local Dirichlet matrix associated with the positive Helmholtz bilinear form b_{Ω_s} ,
- \tilde{B}_s is the local Neumann matrix associated with the positive Helmholtz bilinear form $b_{\tilde{\Omega}_s}$,
- \hat{A}_s^{-1} corresponds to the local Robin problem on Ω_s .

This eigenproblem is written under the assumption of no Dirichlet boundary conditions ($\Gamma_D = \emptyset$) for simplicity, but can accommodate them as long as the action of $\hat{A}_s^{-1} R_s \check{R}_s^T \check{A}_s$ yields a solution satisfying the problem boundary conditions.

By construction, this eigenproblem is *self-adjoint and coercive*, so all eigenvalues λ are real and positive. Moreover, while B_s and \tilde{B}_s are typically associated with the positive Helmholtz matrix, other SPD matrices could also be used in their place. We point out that the matrix on the right-hand side does not have to be assembled in practice to solve the eigenproblems; it is enough to know the matrix-vector product.

The coarse space basis is formed by collecting all vectors of the form

$$Z = \left\{ R_s^T D_s \left(R_s \check{R}_s^T - \hat{A}_s^{-1} R_s \check{R}_s^T \check{A}_s \right) \check{\mathbf{u}} : \lambda < \tau \right\}$$

for some user-defined threshold $\tau > 0$. By construction, each resulting vector lies in the global finite element space and corresponds to a *local discrete Helmholtz solution* on Ω_s thanks to the presence of the operator $R_s \check{R}_s^T - \hat{A}_s^{-1} R_s \check{R}_s^T \check{A}_s$, and multiplied by the partition of unity D_s .

4.4 Summary and comparison of spectral coarse spaces

Having described the main families of spectral coarse spaces—namely the DtN, GenEO-type, and Helmholtz-harmonic constructions—we now highlight their connections and comparative features. A summary of this comparison is given in Table 1.

Conceptual links Despite differing technical constructions, all approaches share a common spectral philosophy: they extract low-energy components via localised eigenproblems, then assemble them into globally supported basis functions using a partition of unity.

The **DtN** coarse space is the most geometrically minimal, using interface-local eigenfunctions extended via Helmholtz harmonic continuation. In this sense, it belongs to the broader class of **Helmholtz-harmonic coarse spaces**. It may also be seen as a precursor to the **GenEO** family, which replaces boundary-local eigenproblems with volumetric ones defined over subdomains or overlapping regions. The **harmonic GenEO** spaces, in turn, reinterpret the GenEO framework by restricting the usual self-adjoint positive definite eigenproblems to the subspace of local Helmholtz solutions. The constraint to solve in the Helmholtz-harmonic subspace can be imposed using an augmented eigenproblem. Finally, the **extended-harmonic** coarse spaces involve self-adjoint positive definite eigenproblems similarly to the GenEO family, but posed on an extended subdomain and with a suitable operator weighting the matrix in the eigenproblem. The resulting eigenvectors are projected in the Helmholtz-harmonic subspace of the (non-extended) subdomain.

Complexity comparison The main costs of two-level domain decomposition preconditioners are: (i) construction of the coarse space (local eigenproblems and global assembly), (ii) factorisation of the coarse operator, and (iii) repeated local and coarse solves during GMRES iterations.

For discretisations with a fixed number of points per wavelength ($hk = \mathcal{O}(1)$) as often happens in engineering practice, the number of unknowns per subdomain scales like $\mathcal{O}(k^d)$ in d dimensions, while the number of unknowns on the subdomain boundary scales like $\mathcal{O}(k^{d-1})$. As a result the cost of constructing the coarse space and its dimension differ between the different methods:

- **DtN:** the eigenproblem is posed on the interface (although the operator features a local volume inverse of size $\mathcal{O}(k^d)$) and as a result, the number of basis functions is bounded by the number of interface unknowns in $\mathcal{O}(k^{d-1})$.
- **GenEO-type:** the eigenproblem is volumetric hence leads to $\mathcal{O}(k^d)$ candidate functions per subdomain. To ensure wavenumber-independent convergence, the coarse operator (although well below this limit in practice) can become large, leading to an important factorisation cost.
- **Harmonic:** The saddle-point eigenproblem is twice the number of unknowns in the subdomain, hence of size $\mathcal{O}(k^d)$, but the retained modes need to solve the Helmholtz problem, hence their number is necessarily bounded by the number of boundary unknowns in $\mathcal{O}(k^{d-1})$.
- **Extended harmonic:** The eigenproblem is posed in the extended volume, still in $\mathcal{O}(k^d)$, but the elements in the coarse space are Helmholtz solutions by construction (up to the partition of unity), hence their number is also necessarily bounded by the number of boundary unknowns in $\mathcal{O}(k^{d-1})$.

At runtime, each GMRES iteration requires local subdomain solves (local matrices are factored in the setup phase) typically via sparse direct solvers and a global coarse correction ($\mathcal{O}(N_c^2)$ after factorisation). In principle, these scalings suggest coarse space dimensions increase dramatically with the wavenumber, but in practice our numerical results show milder growth, with iteration counts nearly independent of k once a suitable coarse space is included.

Table 1: Comparison of spectral coarse space families for the Helmholtz problem

Property	DtN	GenEO-type	Harmonic	Extended harmonic
Eigenfunctions	Interface Γ_s	Subdomain Ω_s (or overlap)	Subdomain Ω_s	Extended subdomain $\tilde{\Omega}_s$
Spectral domain	Interface	Full volume	Helmholtz-harmonic subspace	Full extended volume
Eigenvalues	complex	complex	real positive	real positive
Maximum dimension	$\mathcal{O}(\Gamma_s)$	$\mathcal{O}(\Omega_s)$	$\mathcal{O}(\Gamma_s)$	$\mathcal{O}(\Gamma_s)$
Theory	None (empirically)	Available for some variants	Available	Available
Adapted to high k	Yes	Yes (H_k -GenEO)	Yes	Yes
Notable references	[14]	[46], [9], [16], [13]	[38], [42]	[43]

Rationale for numerical comparison Given the subtle theoretical distinctions and the absence of definitive complexity bounds in the indefinite Helmholtz regime, it is difficult to draw conclusions purely from the analytical form of the coarse spaces. The actual performance depends on practical implementation details, the choice of eigenvalue threshold, and the frequency regime. Therefore, a numerical comparison is essential to:

- assess the robustness of each coarse space across a range of frequencies and heterogeneous media;
- quantify the trade-off between coarse space dimension and solver convergence;
- validate whether the observed empirical behaviour aligns with or diverges from existing theoretical predictions.

In the next section, we provide such a numerical study, focusing on both homogeneous and heterogeneous Helmholtz problems with increasing complexity.

5 Numerical assessment and comparison

The purpose of this section is to evaluate the performance and robustness of the spectral coarse spaces introduced in Section 4 in realistic simulation settings. While these methods differ in their mathematical formulation and spectral construction, it is often difficult to draw firm conclusions about their practical efficiency based solely on theoretical arguments. In particular, the coarse space dimension, conditioning effects, and preconditioner performance depend intricately on the frequency, domain geometry, heterogeneity, and the choice of eigenvalue threshold.

To overcome this, we conduct a series of numerical experiments designed to probe the behaviour of each coarse space under increasing complexity evaluated within a common two-level ORAS preconditioning framework, using GMRES as the iterative solver. In all cases, the GMRES solver is not restarted and the tolerance is 10^{-6} on the residual, with a right-preconditioning. The overlap is minimal (unless stated otherwise) with a symmetry constraint with respect to the interface, implying two layers of cells in the overlap. Each test case is analysed through a combination of strong and weak scaling experiments, studying the influence of:

- subdomain diameter (in wavelength),
- coarse space size (global and per subdomain),
- eigenvalue threshold τ ,
- and overlap and partition of unity choices.

Our goal is to assess both efficiency (number of GMRES iterations) and scalability (coarse space dimension and distribution), and to offer a fair comparison between the different coarse space strategies under practically relevant conditions.

Implementation details The FreeFEM implementation of the benchmarks is done within the `ffddm` framework, a set of parallel FreeFEM scripts implementing Schwarz domain decomposition methods. The `ffddm` documentation is available on the FreeFem.org web page (see [48]). The `ffddm` framework relies on Message Passing Interface (MPI) parallelism. As is usually done in domain decomposition methods, we assign one subdomain per MPI process.

The first step is to decompose the computational domain into overlapping subdomains. Unless otherwise stated, the automatic graph partitioner Metis [40] is used, which produces a non-overlapping decomposition of the set of mesh elements while minimising interfaces between subdomains and conserving good load-balancing. The overlapping decomposition is then obtained by adding successive layers of elements to reach the desired size of overlap. The setup of the one-level preconditioner then consists in assembling and factorising the local matrices in each subdomain in parallel. This is done using the sparse direct solver MUMPS [2]. The two-level preconditioner for each method is then built by first solving the corresponding local eigenvalue problems in each subdomain with SLEPc [37], and finally assembling and factorising the coarse space operator in a distributed manner by MUMPS using a few cores (ranging from 1 to 144 depending on the size of the coarse space).

During the solution phase, each application of the preconditioner involves solving linear systems with local subdomain matrices (first level) and with the coarse space matrix (second level), which is done by forward-backward substitution using the factorisations computed during the setup phase.

A FreeFEM script comparing all methods for the homogeneous Helmholtz equation in a square is available at <https://github.com/FreeFem/FreeFem-sources/blob/develop/examples/ffddm/Helmholtz-2d-all.edp>.

5.1 Numerical simulations in a square: homogeneous and heterogeneous problems

The numerical tests in this section are structured as follows:

1. **Homogeneous test case.** A baseline benchmark on a unit square domain with Robin boundary conditions and a single interior point source. This allows us to measure the scaling of coarse space dimension and iteration count with respect to the number of subdomains and frequency, in a basic controlled setting.
2. **Heterogeneous test case.** A layered medium with strong contrasts in wave speed is introduced to study robustness under medium heterogeneity and its impact on coarse space size and convergence.

5.1.1 Homogeneous problem

In this part we base the numerical experiments on the model problem in 2D, defined on the unit square $\Omega = (0, 1)^2$. We impose Robin boundary conditions on all sides of the domain. A point source is located in the centre of the domain at $(\frac{1}{2}, \frac{1}{2})$ and provides the forcing function f . The point source is numerically modelled by a Gaussian function: $f(x, y) = 10^4 \exp(-10^3[(x - \frac{1}{2})^2 + (y - \frac{1}{2})^2])$. A schematic of this model problem is found in Figure 1.

To discretise the problem, we triangulate Ω using a Cartesian grid with spacing h and alternating diagonals to form a simplicial mesh. We consider constant coefficients $a(\mathbf{x}) \equiv 1$ and $m(\mathbf{x}) \equiv 1$. The local wavenumber $k = \omega \sqrt{\frac{m}{a}} = \omega$ is then constant and the wavelength used to measure geometrical parameters is $\lambda_{\min} = 2\pi/k$. The discrete problem (2.5) is assembled using a \mathbb{P}_2 finite element approximation on this mesh. To mitigate the *pollution effect*, we choose the angular frequency ω (or equivalently the wavenumber k) and the mesh size h simultaneously so that the dimensionless quantity kh remains sufficiently small. In practice, this is enforced by fixing a minimum number of grid points per wavelength λ_{\min} ; here, we ensure that $kh \lesssim 0.5$, which corresponds to at least 10 points per wavelength λ_{\min} .

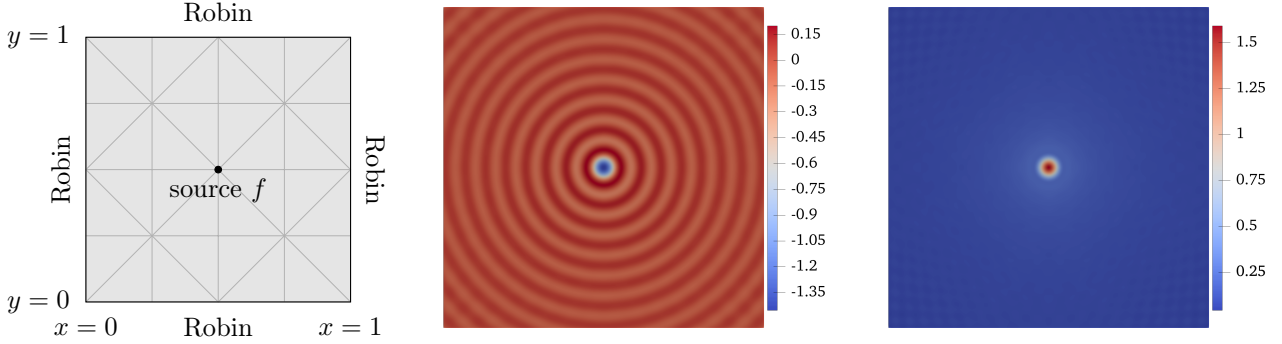


Figure 1: Schematic of the 2D wave guide model problem with example triangular mesh. Real part (left) and modulus (right) of the total field for the homogeneous media test case with $\omega = 100$.

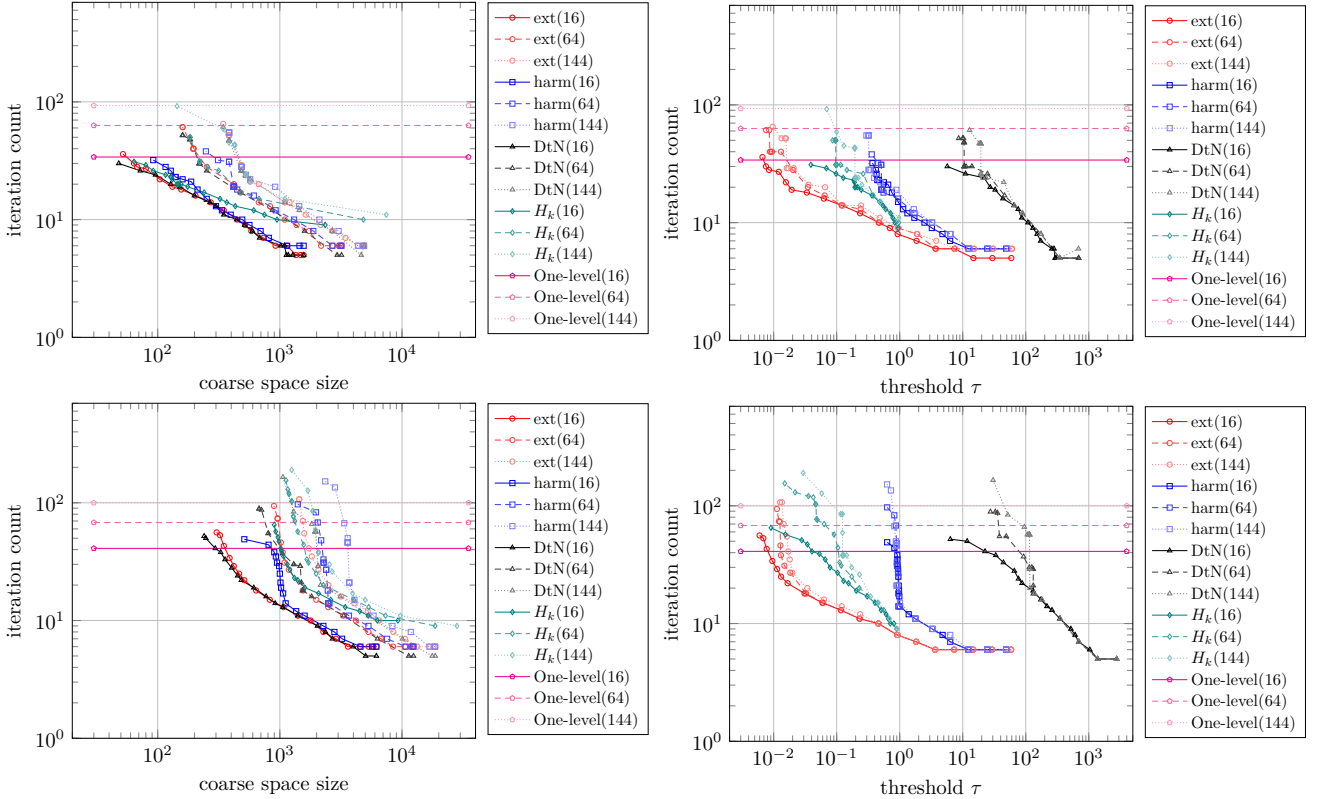


Figure 2: Influence of the coarse space size (left) and threshold choice (right) on the iteration count in strong scaling for the homogeneous media test case with $\omega = 20$ (top) and $\omega = 100$ (bottom). The number in brackets indicates the number of subdomains.

L	λ_{\min}	N	n	H	λ_{\min}	n_s	$n_s^{\partial\Omega_s}$	llvl	ext			harm			DtN			H_k		
								It	It	CS	CS _s	It	CS	CS _s	It	CS	CS _s	It	CS	CS _s
4.5	16	231361	1.1	15373	490	34	5	1352	84	6	1148	72	5	1132	71	9	2352	147		
4.5	36	231361	0.8	7108	331	47	6	1528	42	6	1904	53	5	2102	58	10	3576	99		
4.5	64	231361	0.6	4156	251	63	6	2176	34	6	2690	42	5	2946	46	10	4832	76		
4.5	100	231361	0.5	2762	203	77	6	2784	28	6	3504	35	5	3802	38	11	6094	61		
4.5	144	231361	0.4	1990	171	93	6	4368	30	6	4366	30	5	4636	32	11	7440	52		
9.0	16	519841	2.3	33853	730	36	6	1360	85	6	1724	108	5	1906	119	9	3504	219		
9.0	36	519841	1.5	15455	491	48	6	2298	64	6	2864	80	5	3116	87	10	5304	147		
9.0	64	519841	1.1	8926	371	63	6	3200	50	6	3996	62	5	4342	68	10	7136	112		
9.0	100	519841	0.9	5863	299	73	6	5140	51	6	5140	51	5	5572	56	10	8962	90		
9.0	144	519841	0.8	4177	251	92	6	6480	45	6	6478	45	5	6834	47	10	10896	76		
13.5	16	1442401	3.4	92413	1210	39	5	3346	209	6	2856	178	5	3156	197	10	3316	207		
13.5	36	1442401	2.3	41748	811	52	6	4748	132	7	4768	132	6	4182	116	10	8760	243		
13.5	64	1442401	1.7	23866	611	67	6	5316	83	6	6684	104	5	7164	112	10	11744	184		
13.5	100	1442401	1.4	15520	491	82	6	6874	69	6	8576	86	5	9148	91	10	14760	148		
13.5	144	1442401	1.1	10950	411	97	6	8448	59	6	10460	73	5	11186	78	10	17808	124		
18.0	16	2076481	4.5	132493	1450	39	6	3404	213	6	4288	268	7	3782	236	10	6960	435		
18.0	36	2076481	3.0	59695	971	51	6	5676	158	7	5728	159	6	5020	139	10	10488	291		
18.0	64	2076481	2.3	34036	731	67	6	8000	125	7	8028	125	6	7044	110	9	14048	220		
18.0	100	2076481	1.8	22077	587	81	6	8180	82	6	10344	103	5	10950	110	10	17596	176		
18.0	144	2076481	1.5	15537	491	98	6	10074	70	6	13992	97	6	13340	93	10	21264	148		
22.5	16	3690241	5.6	234253	1930	41	6	3616	226	6	4570	286	5	5042	315	10	6280	392		
22.5	36	3690241	3.8	105188	1291	54	6	6036	168	6	7612	211	5	8198	228	9	13944	387		
22.5	64	3690241	2.8	59776	971	68	6	8452	132	6	10692	167	5	11358	177	9	18656	292		
22.5	100	3690241	2.3	38647	779	84	6	14940	149	7	13778	138	6	14526	145	9	23362	234		
22.5	144	3690241	1.9	27110	651	100	6	13344	93	6	16796	117	5	17694	123	9	28176	196		

Table 2: Strong scaling experiment for the homogeneous media test case.

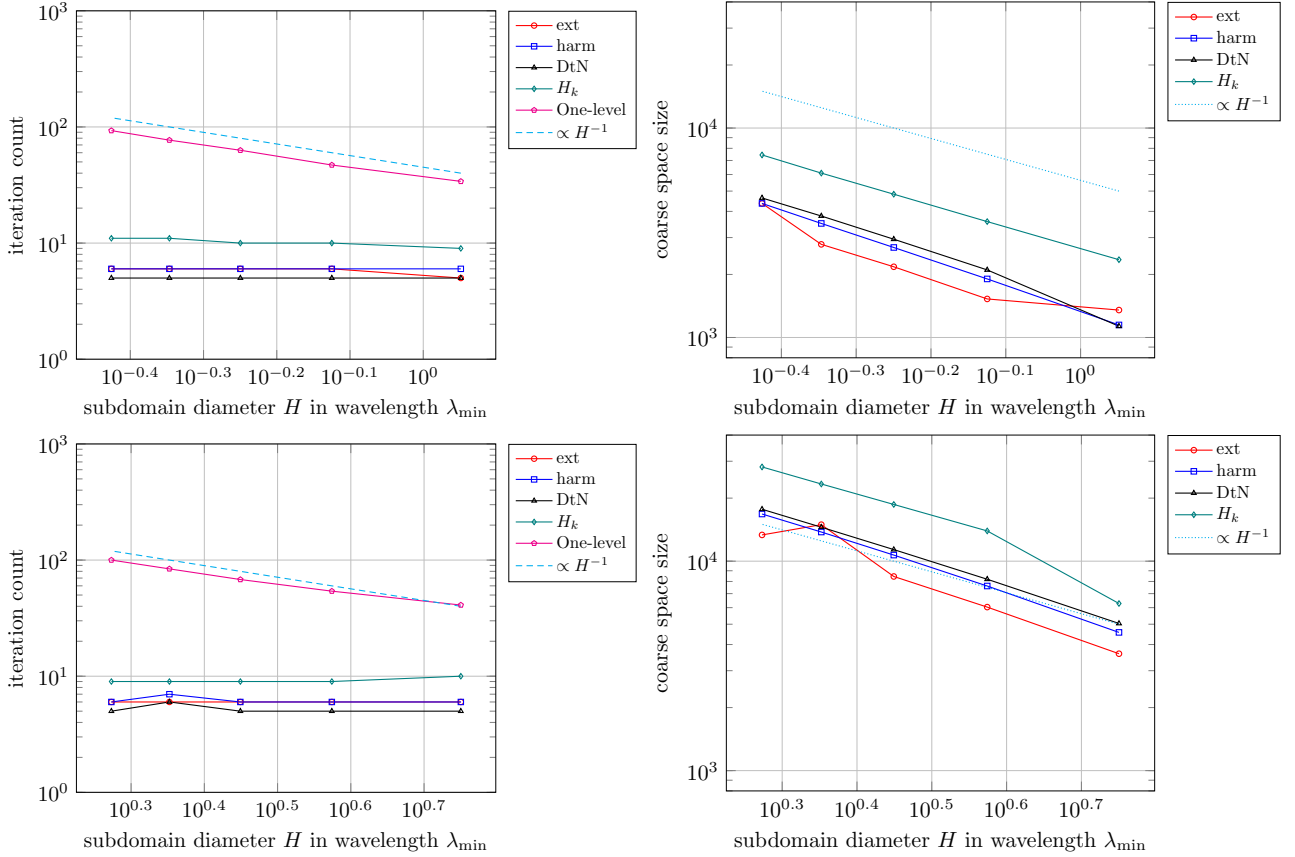


Figure 3: Influence of the subdomain diameter on the iteration count (left) and coarse space size (right) in strong scaling for the homogeneous media test case $\rho = 10$ with $\omega = 20$ (top) and $\omega = 100$ (bottom).

5.1.2 Heterogeneous problem

The next numerical experiments aim to study the robustness of the method with respect to medium heterogeneity. For this purpose, we consider a layered medium in the unit square. More precisely, we use an *alternating layer* configuration (see Figure 4) in which the heterogeneity is introduced through the material parameter $m(\mathbf{x})$. In the present setting, we keep $a(\mathbf{x}) \equiv 1$ everywhere and the mass coefficient is defined as $m(\mathbf{x}) = c(\mathbf{x})^{-2}$, where $c(\mathbf{x})$ is the spatially varying wave speed. The medium alternates between two constant wave speeds: $c(\mathbf{x}) \in \{1, \rho\}$, where $\rho > 1$ is a contrast parameter controlling the strength of the heterogeneity. The local wavenumber is then given by $k(\mathbf{x}) = \omega \sqrt{\frac{m(\mathbf{x})}{a(\mathbf{x})}} = \frac{\omega}{c(\mathbf{x})}$, with $\omega > 0$ the angular frequency. In our numerical experiments, we vary ω while keeping ρ fixed unless otherwise stated. Geometric parameters are measured using the minimal wavelength $\lambda_{\min} = 2\pi/\omega$ corresponding to $c(\mathbf{x}) = 1$. An example of a numerical solution for the heterogeneous layered medium is shown in Figure 4.

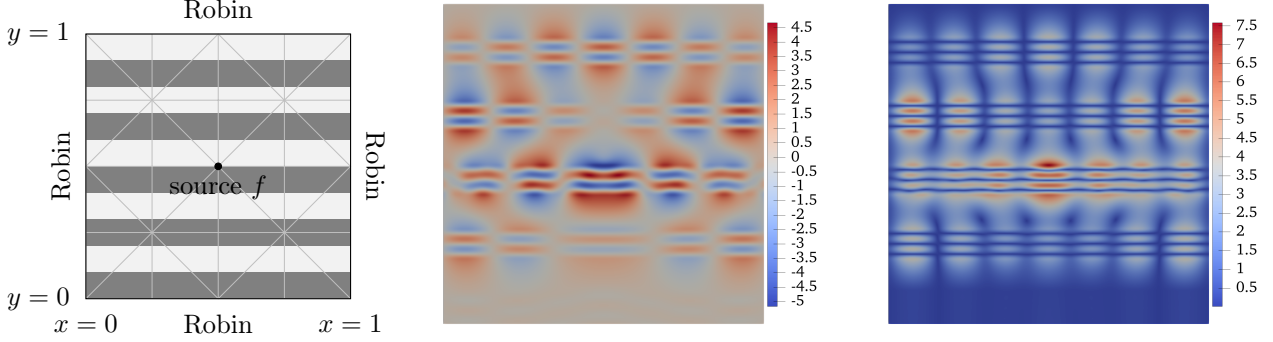


Figure 4: Piecewise constant layer profiles for the wave speed $c(\mathbf{x})$ (left). For the darkest shade, $c(\mathbf{x}) = 1$, while for the lightest shade, $c(\mathbf{x}) = \rho$, with ρ being the contrast factor. Real part (middle) and modulus (right) of the total field for the heterogeneous media test case: $\rho = 10$ and $\omega = 100$.

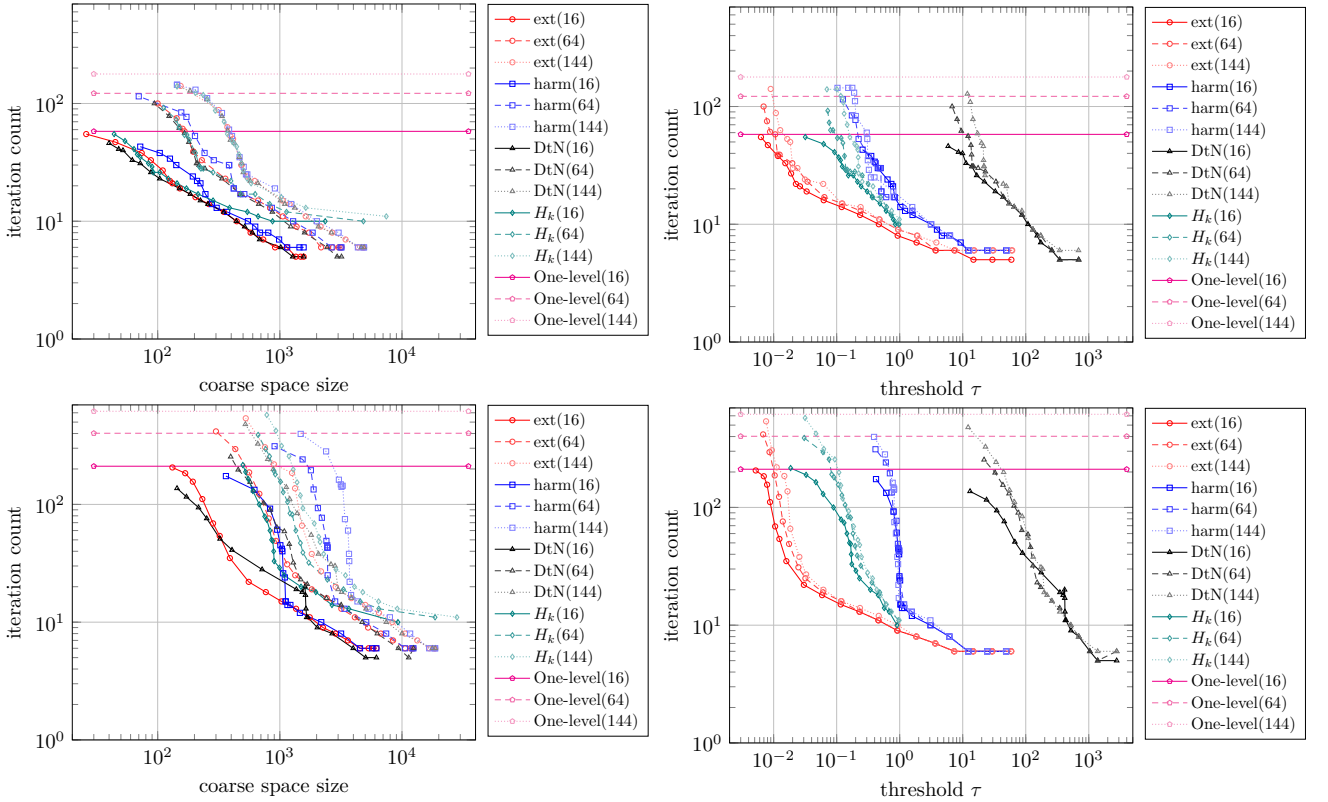


Figure 5: Influence of the coarse space size (left) and threshold choice (right) on the iteration count in strong scaling for the heterogeneous media test case $\rho = 10$ with $\omega = 20$ (top) and $\omega = 100$ (bottom).

L [λ_{\min}]	N	n	H [λ_{\min}]	n_s	$n_s^{\partial\Omega_s}$	llvl	ext			harm			DtN			H_k		
						It	It	CS	CS _s	It	CS	CS _s	It	CS	CS _s	It	CS	CS _s
4.5	16	231361	1.1	15373	490	58	5	1352	84	6	1148	72	5	1276	80	10	872	54
4.5	36	231361	0.8	7108	331	94	6	1528	42	6	1904	53	5	2100	58	10	3576	99
4.5	64	231361	0.6	4156	251	122	6	2176	34	6	2652	41	5	2946	46	10	4832	76
4.5	100	231361	0.5	2762	203	154	6	3500	35	6	3504	35	5	3802	38	11	6094	61
4.5	144	231361	0.4	1990	171	178	6	4368	30	6	4356	30	6	4636	32	11	7440	52
9.0	16	519841	2.3	33853	730	119	6	1710	107	6	1712	107	5	1906	119	10	3504	219
9.0	36	519841	1.5	15455	491	178	6	2860	79	6	2864	80	6	2538	70	11	5304	147
9.0	64	519841	1.1	8926	371	231	6	4032	63	6	4644	73	6	3572	56	11	7136	112
9.0	100	519841	0.9	5863	299	294	6	5140	51	6	5924	59	6	5572	56	11	8962	90
9.0	144	519841	0.8	4177	251	327	6	6409	45	6	7137	50	6	5764	40	12	10896	76
13.5	16	1442401	3.4	92413	1210	84	5	3345	209	6	2838	177	5	3154	197	10	5808	363
13.5	36	1442401	2.3	41748	811	117	5	5372	149	6	4732	131	6	4177	116	10	8760	243
13.5	64	1442401	1.7	23866	611	157	7	6657	104	8	6660	104	13	3956	62	10	11744	184
13.5	100	1442401	1.4	15520	491	205	6	6848	68	6	8560	86	5	9148	91	10	14760	148
13.5	144	1442401	1.1	10950	411	198	6	8388	58	6	10460	73	5	11186	78	10	17808	124
18.0	16	2076481	4.5	132493	1450	120	6	3395	212	6	3404	213	8	3778	236	10	6960	435
18.0	36	2076481	3.0	59695	971	160	6	5676	158	7	5676	158	9	6165	171	10	10488	291
18.0	64	2076481	2.3	34036	731	218	6	7964	124	7	7946	124	11	8562	134	10	14048	220
18.0	100	2076481	1.8	22077	587	294	6	10196	102	6	10196	102	5	10948	109	10	17596	176
18.0	144	2076481	1.5	15537	491	288	6	12561	87	6	13992	97	6	13340	93	10	21264	148
22.5	16	3690241	5.6	234253	1930	211	6	4520	282	6	4532	283	5	5039	315	10	9264	579
22.5	36	3690241	3.8	105188	1291	306	6	6014	167	6	7544	210	5	8198	228	10	13944	387
22.5	64	3690241	2.8	59776	971	402	6	10592	166	6	10592	166	5	11357	177	11	18656	292
22.5	100	3690241	2.3	38647	779	553	9	10826	108	8	15407	154	7	14526	145	10	23362	234
22.5	144	3690241	1.9	27110	651	618	6	16754	116	6	16704	116	6	17693	123	11	28176	196

Table 3: Strong scaling experiment for the heterogeneous media test case $\rho = 10$.

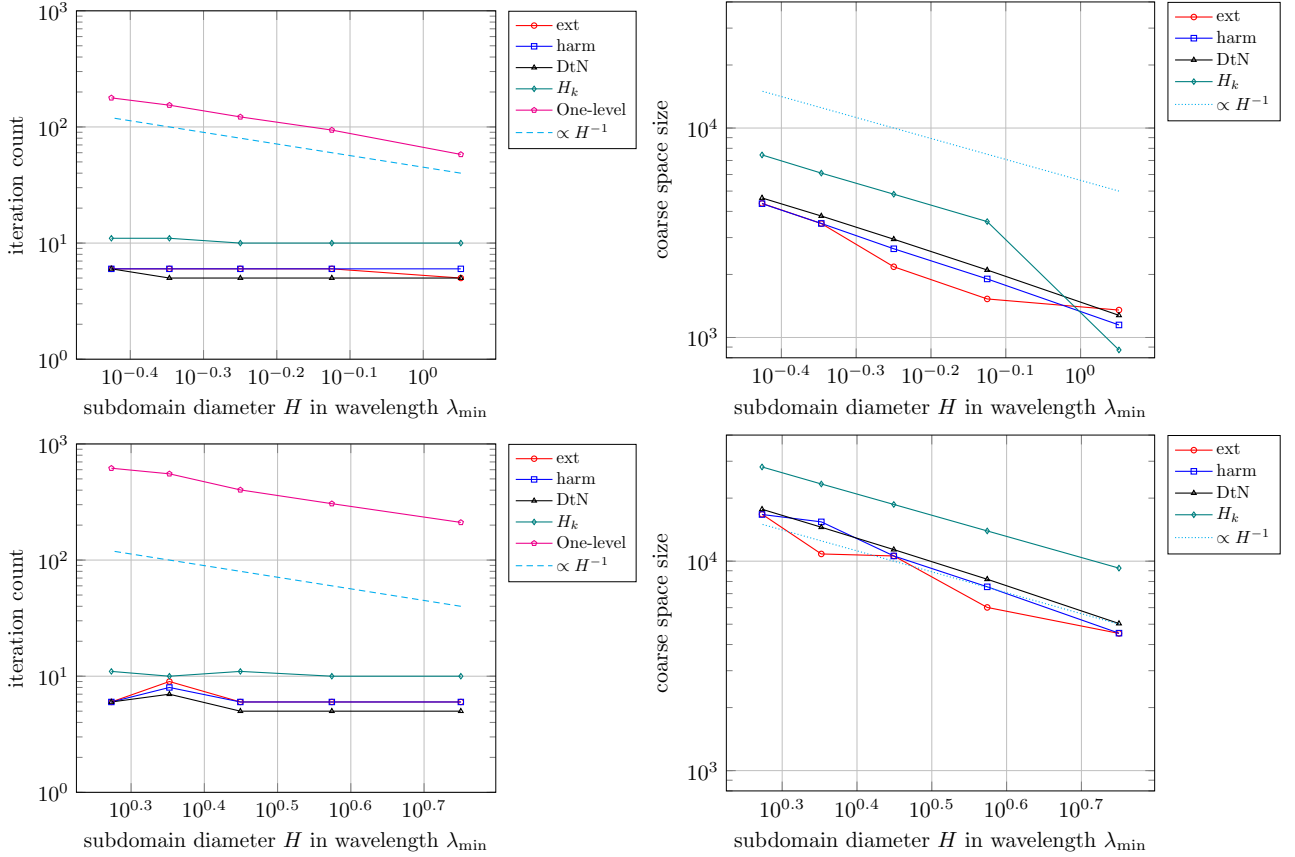


Figure 6: Influence of the subdomain diameter on the iteration count (left) and coarse space size (right) in strong scaling for the heterogeneous media test case $\rho = 10$ with $\omega = 20$ (top) and $\omega = 100$ (bottom).

5.1.3 Results

The full results are provided in Tables 2 and 3. The entries are the diameter of the domain L measured in the smallest wavelength $\lambda_{\min} = 2\pi \min_{\mathbf{x}}(c(\mathbf{x}))/\omega$ present in the problem, the total number of degrees of freedom n , the averaged diameter of a subdomain H measured in wavelength λ_{\min} , the averaged number n_s of degrees of freedom in a subdomain, the averaged number $n_s^{\partial\Omega_s}$ of degrees of freedom on the boundary of a subdomain, the number N of subdomains, the total size of the coarse space (CS), the averaged number of contributions of a subdomain to the coarse space (CS_s) and the number of GMRES iterations to reach the tolerance (It). The methods being

compared are the baseline one-level method (1lvl): extended (ext) and harmonic coarse spaces (harm) on one side with the classical the Dirichlet-to-Neumann (DtN) and H_k -GenEO methods (H_k) on the other side.

Besides, we report, for the smallest and largest frequencies tested, the number of GMRES iterations to reach the required tolerance as a function of the total coarse space size and choice of threshold parameter in Figures 2 and 5. The number of subdomains is provided in brackets in the legend entries. The results reported in the table correspond to the parameters with the minimum number of iterations obtained for each method.

The number of iterations of GMRES to reach the required tolerance as a function of the subdomain diameter (measured in wavelength) is reported Figures 3 and 6.

5.1.4 Assessment and comparative conclusions for the square test cases

We now draw conclusions from the strong scaling tests performed on the 2D square homogeneous and heterogeneous test cases. From both Tables 2–3 and Figures 2–6, several trends emerge consistently across frequencies and levels of heterogeneity. General comments on one-level and two-level methods are:

- The performance of the one-level method deteriorates with increasing frequency or with heterogeneities.
- In contrast, all two-level methods are scalable and very robust with respect to the frequency or in the presence of heterogeneity. As a result, they dramatically outperform the one-level baseline.
- These properties are however achieved only for large enough coarse spaces, as the iteration count of two-level methods correlates strongly with coarse space size.
- In particular, robustness is achieved with a coarse space size that increases with increasing number of subdomains and increasing frequency.

Comparing the different two-level methods, we remark that:

- The smallest number of iterations is achieved with the DtN coarse spaces, closely followed by the harmonic and extended-harmonic coarse spaces, and then by the H_k -GenEO coarse spaces.
- To achieve this, the DtN coarse spaces are however slightly larger than the harmonic and extended-harmonic ones, while the H_k -GenEO coarse spaces are the largest.
- In a context with a tight coarse space size budget, the DtN and extended-harmonic coarse spaces are the most efficient, especially at large frequencies.
- A sensible choice for the eigenvalue threshold τ to ensure low iteration count is in the range 5 – 10 for extended-harmonic, around 10 for harmonic, in the range 500 – 1000 for DtN and in the range 0.8 – 1 for H_k -GenEO.

5.2 A test case from medical imaging

Description of the problem We consider the problem of plane wave scattering by randomly positioned, penetrable micro-reflectors in two dimensions. This setting models acoustic wave interaction with soft biological tissues, as explored in recent quantitative ultrasound imaging studies [28, 29]. We fix a constant *reference medium* with coefficients $a_0 > 0$, $m_0 > 0$, and define the *reference wave speed* and the corresponding *reference wavenumber* and *reference wavelength*

$$c_0 = \sqrt{\frac{a_0}{m_0}}, \quad k_0 = \omega \sqrt{\frac{m_0}{a_0}} = \frac{\omega}{c_0}, \quad \lambda_0 = \frac{2\pi}{k_0}.$$

All geometric parameters in this test case will be expressed in units of λ_0 .

The incident wave is a plane wave of the form $u_i(\mathbf{x}) = \exp(i k_0 \mathbf{d} \cdot \mathbf{x})$, $\mathbf{d} \in \mathbb{R}^2$, $|\mathbf{d}| = 1$, where \mathbf{d} is the propagation direction. The total field u satisfies the heterogeneous Helmholtz equation

$$-\nabla \cdot (a(\mathbf{x}) \nabla u) - \omega^2 m(\mathbf{x}) u = 0, \quad \text{in } \mathbb{R}^2,$$

with an outgoing radiation condition on the scattered field $u_s = u - u_i$. The coefficients $a(\mathbf{x})$ and $m(\mathbf{x})$ describe the $N_r \in \mathbb{N}$ penetrable micro-reflectors:

$$a(\mathbf{x}) = \mathbf{1}_{\Omega \setminus \bigcup_{j=1}^{N_r} B_\epsilon(\mathbf{x}_j)} + \sum_{j=1}^{N_r} a_j \mathbf{1}_{B_\epsilon(\mathbf{x}_j)}, \quad c_0^2 m(\mathbf{x}) = \mathbf{1}_{\Omega \setminus \bigcup_{j=1}^{N_r} B_\epsilon(\mathbf{x}_j)} + \sum_{j=1}^{N_r} m_j \mathbf{1}_{B_\epsilon(\mathbf{x}_j)}, \quad (5.1)$$

where $B_\epsilon(\mathbf{x}_j)$ is a disk of radius $\epsilon = \lambda_0/4$ centred at \mathbf{x}_j , a_j and m_j are drawn from a normal distribution with mean 1 and standard deviation $\sigma = 0.1$, the disk centres \mathbf{x}_j are generated by a Matérn hardcore spatial process. In the background medium (a_0, m_0) we have $k(\mathbf{x}) \equiv k_0$, while inside each inclusion $k(\mathbf{x})$ deviates due to the perturbed material parameters.

We truncate the unbounded domain using a perfectly matched layer (PML) following [25]. Let $\chi \in C_{\text{comp}}^\infty(\mathbb{R}^2)$ be a smooth cut-off function supported around the heterogeneous region that is identically one on an open connected set including the support of $(1 - m)(1 - a)$. We introduce the compactly supported unknown

$$\tilde{u} := u - (1 - \chi)u_i,$$

which satisfies

$$-\nabla \cdot (a(\mathbf{x})\nabla \tilde{u}) - \omega^2 m(\mathbf{x}) \tilde{u} = 2 \nabla \chi \cdot \nabla u_i + u_i \Delta \chi, \quad \text{in } \mathbb{R}^2.$$

We use a PML implementation adapted from [5].

A snapshot of the medium and computed fields is shown in Figure 7 for $N_r = 2040$ reflectors in a domain of size $47.8\lambda_0 \times 47.8\lambda_0$. The presence of the micro-reflectors imposes a strong constraint on the mesh size corresponding to about 22 points per wavelength λ_0 . We use \mathbb{P}_2 Lagrange finite elements.

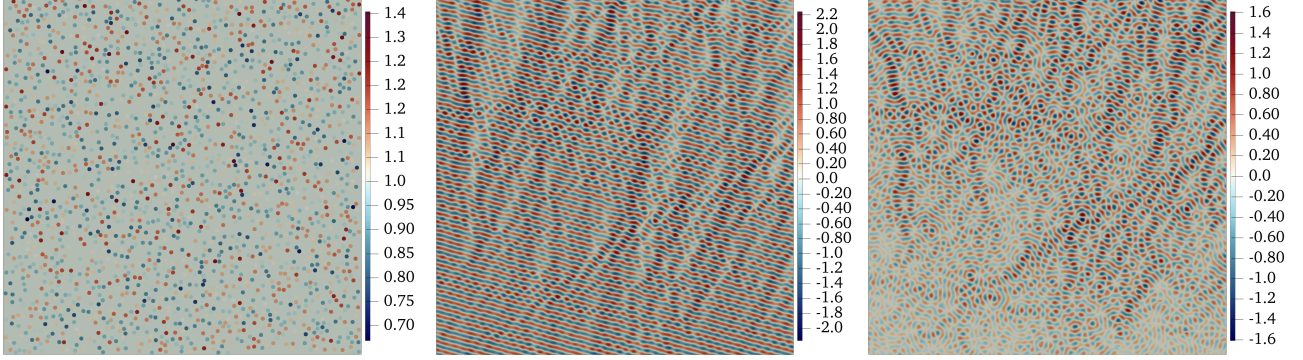


Figure 7: Values of the coefficient $c_0^2 m$ (left), real part of total field $\text{Re}(u)$ (middle), and real part of scattered field $\text{Re}(u_s)$ (right).

Strong scaling test We first provide results for a strong scaling test, increasing the number of subdomains for a fixed problem size. The full domain has size $23.9\lambda_0 \times 23.9\lambda_0$ with 1213761 DOFs. The full results are provided in Table 4. The entries are the same as the ones previously described, except we use the reference wavelength λ_0 to measure lengths. Besides, we report the number of iterations of GMRES to reach the required tolerance as a function of the total coarse space size and choice of threshold parameter in Figure 8. The number of subdomains is provided in brackets in the legend entries. The results reported in the table correspond to the parameters with the minimum number of iterations obtained for each method, which explains the difference for the DtN approach. The number of iterations of GMRES to reach the required tolerance as a function of the subdomain diameter (measured in wavelength) is reported Figure 9.

Weak scaling test We then perform a weak scaling test, increasing the number of subdomains for a fixed subdomain size. Each subdomain is in average of size $4.2\lambda_0 \times 4.2\lambda_0$ with about 39000 DOFs. The mesh size is fixed, so the pollution effect is not taken into account. The full results are provided in Table 5 with the same entries as for the strong scaling test case. The number of iterations of GMRES to reach the required tolerance as a function of the total coarse space size and choice of threshold parameter is reported Figure 10. The number of iterations of GMRES to reach the required tolerance as a function of the full domain diameter (measured in wavelength) is reported Figure 11.

Overlap and partition of unity function We turn to the study of the influence of the width of the overlap. So far the results for this test case are obtained for minimal overlap (with a symmetry constraint with respect to the interface). The number of iterations of GMRES to reach the required tolerance as a function of the total coarse space size is reported in Figure 12. The size of the overlap measured as the number of cell layers from one side of the interface is indicated in the brackets of the legend entries.

Three different partition of unity functions, all defined as \mathbb{P}_1 functions hence piecewise affine, are used. The first one is the steepest, going from 1 to 0 in the smallest number of cells (typically two) close to the interface. The second one is the smoothest, going from 1 to 0 on the full size of the overlap. The third one is an intermediate choice, decaying smoothly on the overlap but vanishing one layer of cells before reaching the boundary, hence ensuring that its first derivative vanishes on the boundary (which makes sense in our case since we are using optimised boundary conditions as transmission conditions).

L	$[\lambda_0]$	N	n	H	$[\lambda_0]$	n_s	$n^{\partial\Omega_s}$	1lvl	ext			harm			DtN			H_k		
									It	CS	CS $_s$	It	CS	CS $_s$	It	CS	CS $_s$	It	CS	CS $_s$
33.8	8	1213761	11.9	154757	1664	37	6	2073	259	6	2371	296	12	2663	333	24	3894	487		
33.8	16	1213761	8.4	78134	1121	46	7	2499	156	8	2907	182	16	1807	113	23	5380	336		
33.8	32	1213761	6.0	39751	812	66	7	4456	139	9	5048	158	19	2652	83	21	7791	243		
33.8	64	1213761	4.2	20308	568	83	8	6460	101	11	7098	111	24	2245	35	22	10906	170		
33.8	128	1213761	3.0	10487	413	112	9	8198	64	13	9874	77	26	3564	28	23	15849	124		
33.8	256	1213761	2.1	5454	286	145	10	14222	56	16	14608	57	31	4878	19	24	22005	86		

Table 4: Strong scaling experiment for the imaging test case.

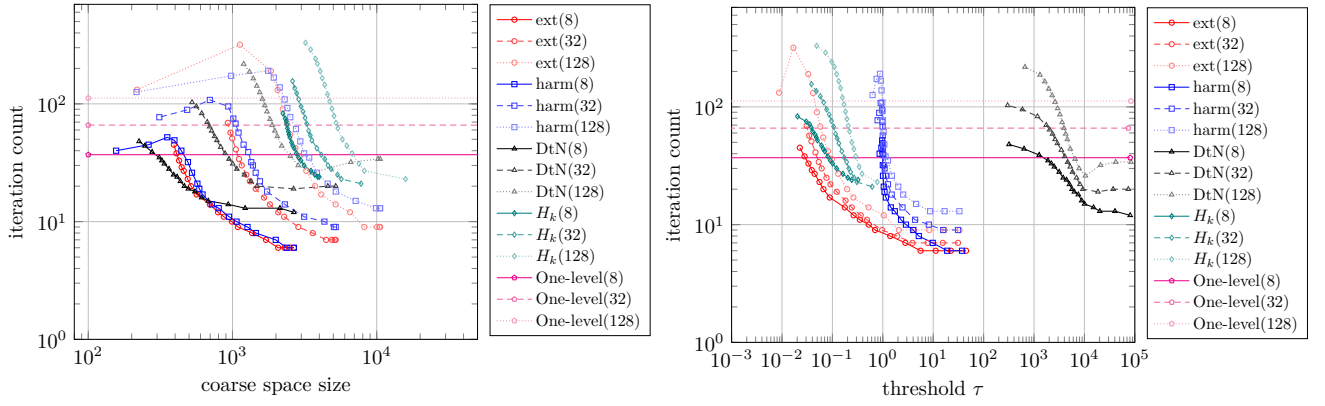


Figure 8: Influence of the coarse space size (left) and threshold choice (right) on the iteration count in strong scaling for the imaging test case.

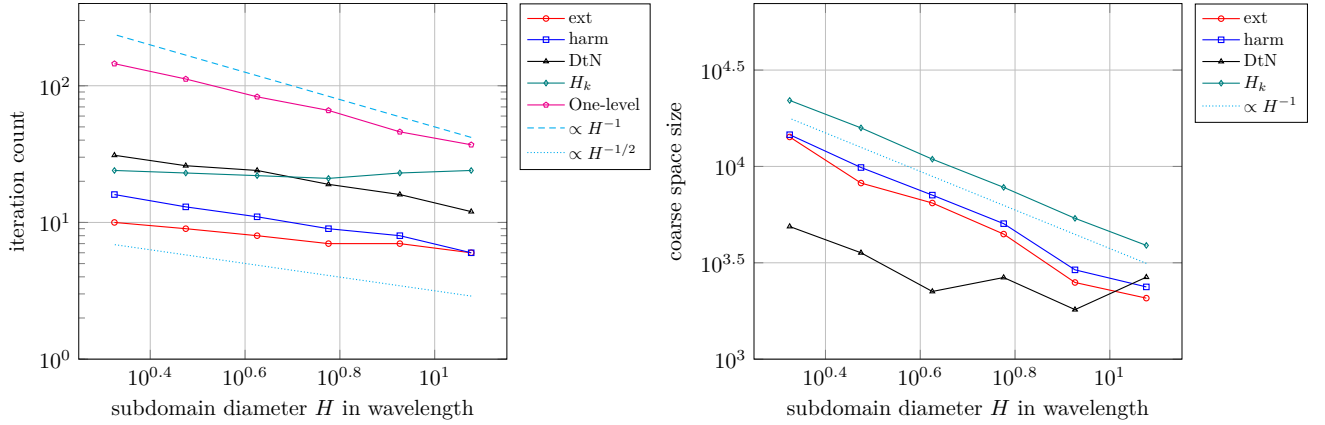


Figure 9: Influence of the subdomain diameter on the iteration count in strong scaling for the imaging test case.

$L [\lambda_0]$	N	n	$H [\lambda_0]$	n_s	$n_s^{\partial\Omega_s}$	llvl	ext			harm			DtN			H_k		
						It	It	CS	CS_s	It	CS	CS_s	It	CS	CS_s	It	CS	CS_s
16.9	8	292873	6.0	38108	829	37	6	1007	126	6	1206	151	12	1060	132	20	1990	249
23.9	16	587129	6.0	38312	792	42	7	2042	128	7	2406	150	16	924	58	22	3804	238
33.8	32	1213761	6.0	39751	812	66	7	4456	139	9	5048	158	19	2652	83	21	7791	243
47.8	64	2366557	6.0	38856	798	86	8	9443	148	11	9288	145	23	5685	89	23	15327	239
67.5	128	4809133	6.0	39573	817	127	9	17250	135	14	19697	154	23	10340	81	23	31375	245
95.5	256	9520591	6.0	39238	811	187	11	39786	155	20	41337	161	29	13850	54	26	62267	243

Table 5: Weak scaling experiment for the imaging test case.

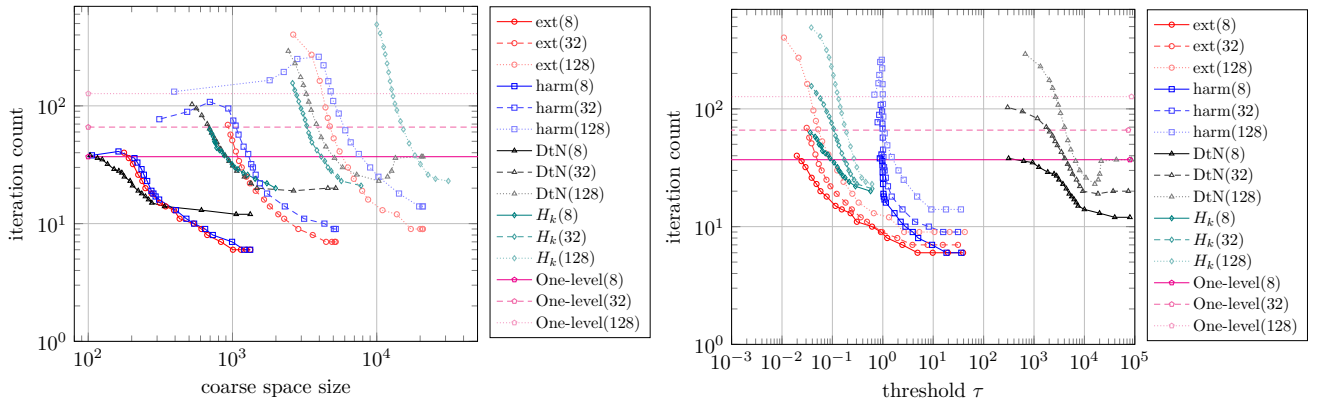


Figure 10: Influence of the coarse space size (left) and threshold choice (right) on the iteration count in weak scaling for the imaging test case.

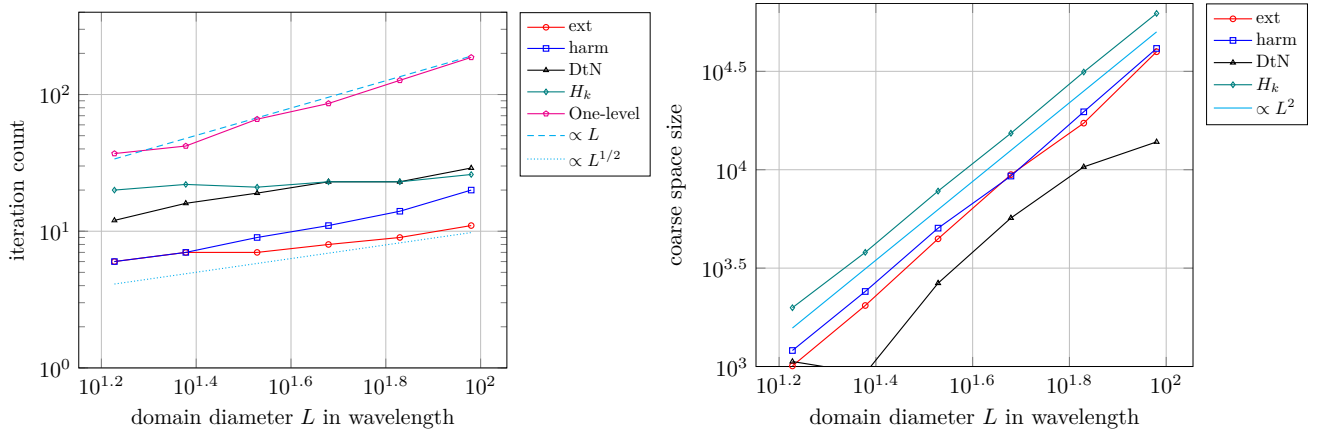


Figure 11: Influence of the full domain diameter on the iteration count in weak scaling for the imaging test case.

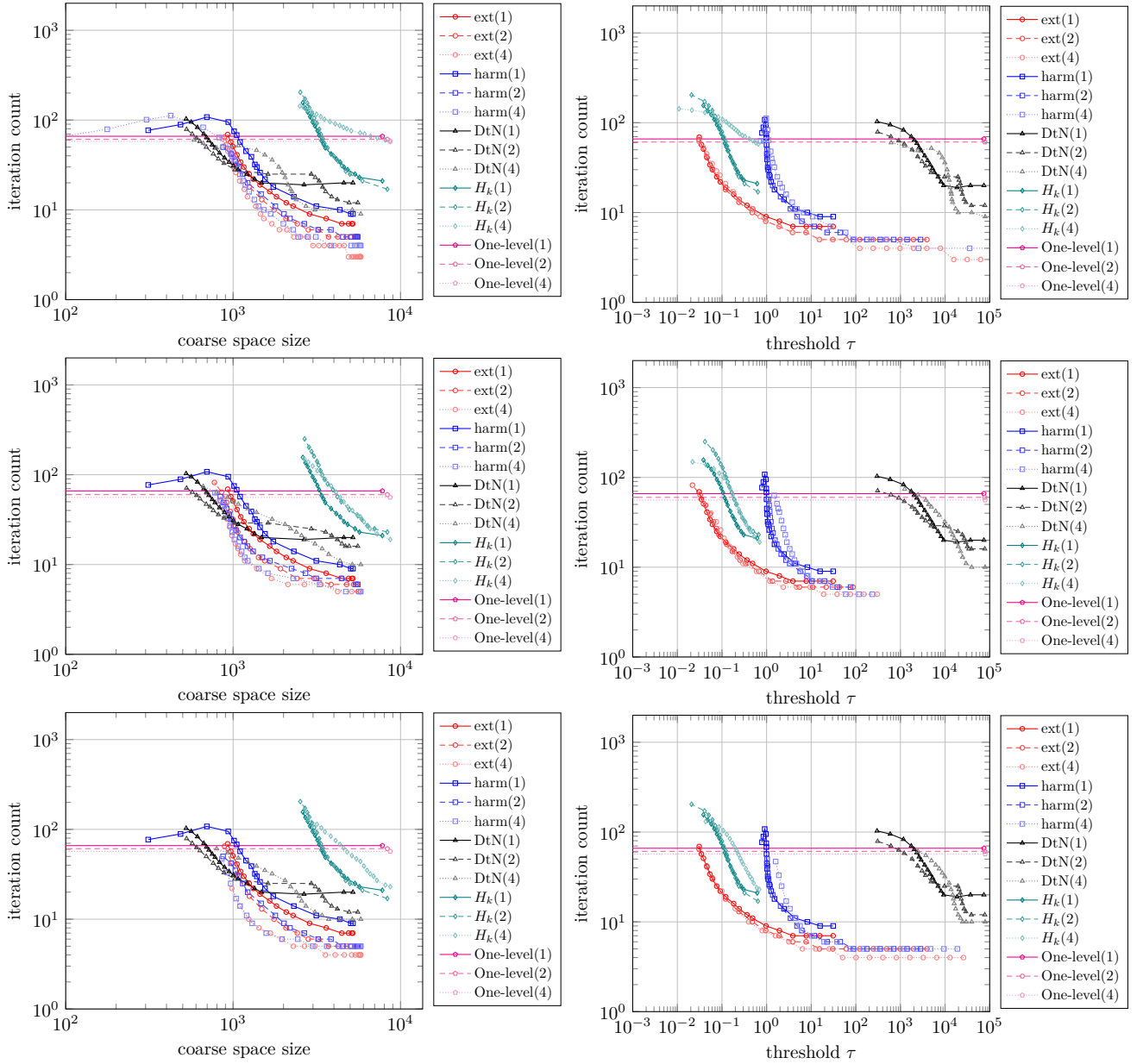


Figure 12: Influence of the overlap and the partition of unity function on the iteration count for the imaging test case. Steep (top), linearly decaying (middle) and with vanishing first derivative on the boundary (bottom).

Assessment and comparative conclusions for the medical imaging test case From these tests we can draw the following conclusions:

- The two-level methods remain robust in both weak and strong scalings, albeit with a moderate increase in the iteration count with the number of subdomains, which is well-controlled by enlarging the coarse space.
- Harmonic and extended-harmonic coarse spaces yield the lowest iteration counts for a given coarse space size, with a slight advantage for the extended harmonic coarse space for larger number of subdomains.
- DtN coarse spaces remain competitive and compact, with a slightly worse iteration count but with the lowest size. We remark however some loss of robustness in the sense that the decrease in the number of iteration is not always monotonic with the size of the coarse space.
- H_k -GenEO coarse spaces are robust but more expensive.
- Sensible choices for the threshold τ are comparable to the previous test case, except for the DtN coarse spaces which required significantly larger values.
- Wider overlaps generally reduce iteration counts, especially for the harmonic and extended-harmonic coarse spaces.
- Smoother partition of unity functions (especially with vanishing derivative) yield slightly better convergence.

The imaging test case highlights the necessity of two-level methods heterogeneous for media with overall performance similar to the simple test on a square domain.

5.3 Cobra cavity test case

Description of the problem We now move to a more sophisticated test case for spectral coarse spaces: the *COBRA cavity*, a three-dimensional, S-shaped waveguide originally designed for electromagnetic scattering studies by EADS Aerospatiale Matra Missiles as part of the EM-JINA 98 workshop (see [39, 41]). This geometry has since been adopted as a benchmark in domain decomposition research (e.g. [17, 6]) due to its challenging features for mid- to high-frequency wave propagation.

Unlike previous test cases with simpler geometries, the COBRA cavity introduces *geometric complexity* through its curvature, which can lead to *wave trapping effects*. Although the wavespeed is constant, the intricate shape of the cavity poses significant numerical challenges that go beyond those of straight waveguides.

The cross-section of the cavity measures $11\text{ cm} \times 8.4\text{ cm}$. The cavity walls are modelled as sound-soft, imposing Dirichlet boundary conditions. To reduce the unbounded scattering domain to a finite computational domain, we embed the cavity in a surrounding box. The material parameters are $a(\mathbf{x}) \equiv 1$ and $m(\mathbf{x}) \equiv 1$ and only the wavenumber k is varied. All geometrical parameters are measured in terms of the wavelength $\lambda = 2\pi/k$. The sides of the box are positioned 10 cm from the cavity in all directions, corresponding to between 1.3 and 5.7 wavelength λ depending on the frequency used in the weak scaling study presented below. Robin (impedance) boundary conditions are applied on all faces of the outer box.

A normally incident plane wave excites the cavity. The problem is discretised using \mathbb{P}_2 Lagrange finite elements, with a resolution of 8 points per wavelength to ensure adequate accuracy in the high-frequency regime.

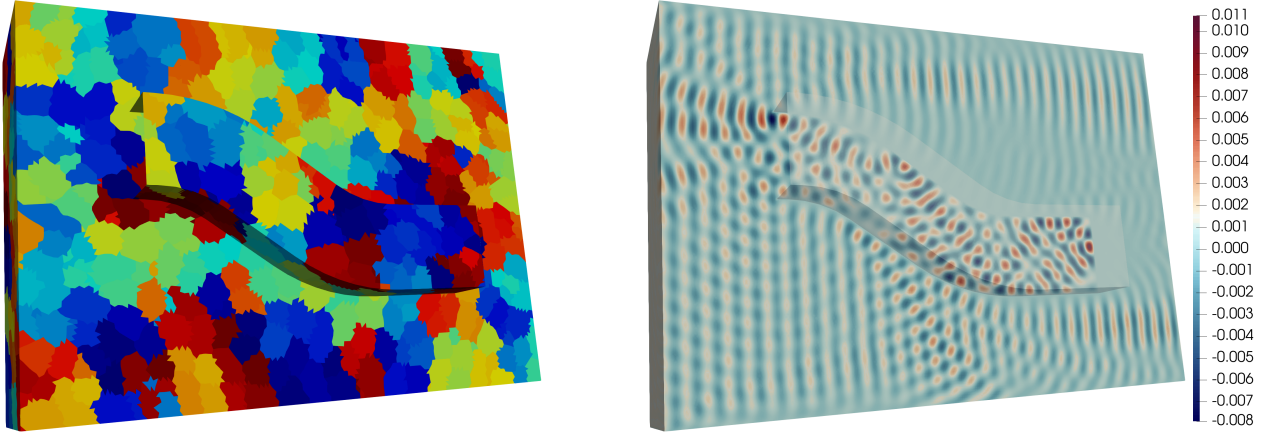


Figure 13: Partitioning of the cobra cavity domain into 2916 subdomains (left) and real part of the total field (right) for $L = 22.9\lambda$ ($k = 360\text{m}^{-1}$).

Weak scaling test To assess scalability in more realistic and complex 3D geometries, we perform a *weak scaling test* on the COBRA cavity benchmark. In this experiment, the number of subdomains and total degrees of freedom increase proportionally with the wavenumber k , while keeping the average *subdomain size fixed* (approximately 1.6 wavelength λ in diameter and around $27,000$ degrees of freedom per subdomain). The number of subdomains N increases from 32 for $k = 80\text{m}^{-1}$ to 2916 for $k = 360\text{m}^{-1}$. Correspondingly, the diameter L of the global domain in wavelength goes from 5.1λ to 22.9λ . As an illustration, Figure 13 shows the partitioning of the domain as well as the real part of the solution for $L = 22.9\lambda$.

As shown in Table 6, the domain diameter measured in wavelengths increases from $L = 5.1\lambda$ (for $N = 32$) up to $L = 22.9\lambda$ (for $N = 2916$). This setup preserves local resolution while increasing the global problem size, making it ideal to evaluate the robustness of coarse spaces and the scalability of the two-level ORAS preconditioner in the mid- to high-frequency regime. In addition to that, we also report the number of GMRES iterations to reach the required tolerance as a function of the total coarse space size and choice of threshold parameter in Figure 14. The number of subdomains is provided in brackets in the legend entries. The number of iterations of GMRES to reach the required tolerance as a function of the full domain diameter (measured in wavelength) is reported in Figure 15.

L [λ]	N	n	H [λ]	n_s	$n_s^{\partial\Omega_s}$	1lvl	ext			harm			DtN			H_k		
						It	It	CS	CS_s	It	CS	CS_s	It	CS	CS_s	It	CS	CS_s
5.1	32	473004	1.6	22336	2986	51	8	6400	200	8	6400	200	13	6400	200	17	6400	200
7.6	108	1761164	1.6	25895	3824	157	10	21600	200	10	21600	200	25	21600	200	38	21600	200
10.2	256	4140366	1.6	26525	4144	359	14	51200	200	12	51200	200	44	51200	200	63	51200	200
12.7	500	8431281	1.6	27980	4468	432	16	100000	200	14	100000	200	64	100000	200	106	100000	200
15.3	864	13927097	1.6	27839	5035	942	34	172800	200	34	172800	200	97	172800	200	>200	172800	200
17.8	1372	18879654	1.6	24589	4676	1055	44	274400	200	46	274400	200	120	274400	200	>200	274400	200
20.4	2048	32848020	1.6	28143	5210	3711	60	409600	200	79	409600	200	162	409600	200	>200	409600	200
22.9	2916	44520439	1.6	27138	5121	3398	74	583200	200	107	583200	200	>200	583200	200	>200	583200	200

Table 6: Weak scaling experiment for the cobra cavity test case.

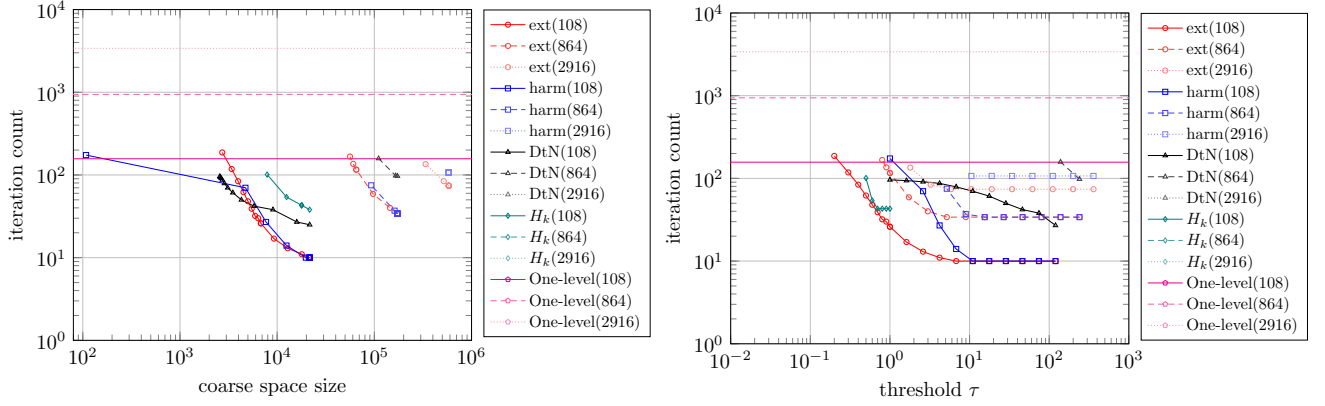


Figure 14: Influence of the coarse space size (left) and threshold choice (right) on the iteration count in weak scaling for the cobra cavity test case.

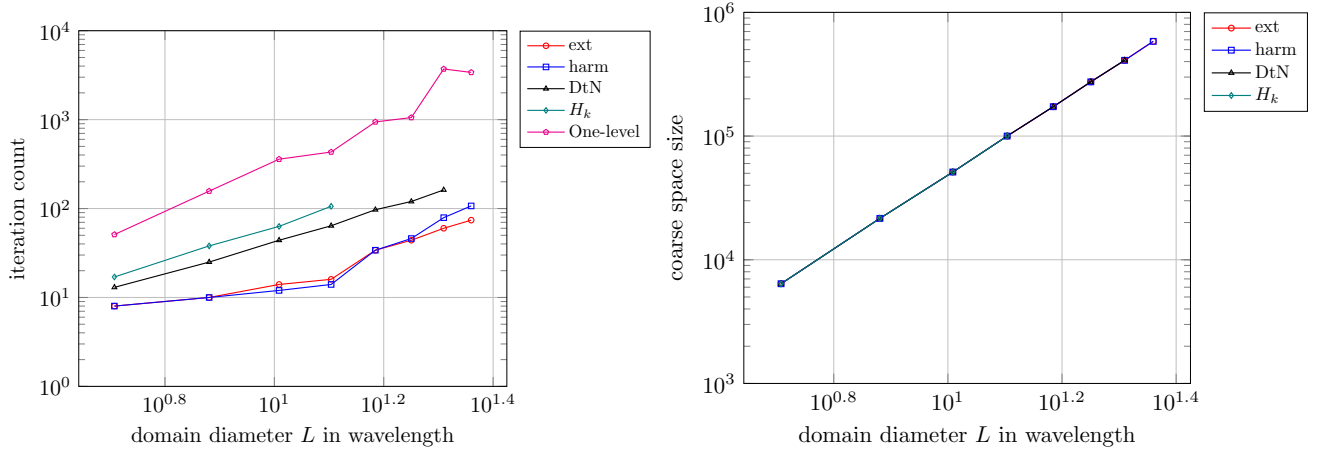


Figure 15: Influence of the full domain diameter on the iteration count in weak scaling for the cobra cavity test case.

Assessment and comparative conclusions for the cobra cavity test case

- GMRES iteration counts show that all two-level methods significantly outperform the one-level baseline, especially as the global domain size L increases.
- Harmonic and extended harmonic coarse spaces consistently achieve the lowest iteration counts, with only mild growth across scales.
- The DtN coarse space performs competitively at moderate scales but exhibits a slight increase in iteration count at higher L , and eventually breaks down for the largest problem.
- H_k -GenEO also performs competitively at moderate scales but breaks down beyond a certain coarse space size and for larger domains.

5.4 The GO_3D_OBS Crustal Geomodel

Description of the problem The GO_3D_OBS crustal geomodel is a high-resolution, three-dimensional synthetic model specifically designed to evaluate seismic imaging techniques, particularly for deep crustal and subduction zone exploration [31]. It represents a continental margin at a regional scale, incorporating realistic geological heterogeneities and sharp velocity contrasts that are characteristic of tectonic plate boundaries.

The model features a wide range of acoustic wavespeeds, $c(\mathbf{x})$ varies from 1500 ms^{-1} in the near-surface sedimentary layers and water column up to 8639 ms^{-1} in the lower crust and upper mantle. This range captures the physical complexity required to simulate realistic wave propagation in crustal-scale full-waveform inversion (FWI) settings.

Importantly, the geomodel includes the essential structural features of subduction zones, such as a dipping slab, accretionary prism, crust-mantle transitions, and bathymetry. It is inspired by a real-world FWI case study performed in the eastern Nankai Trough [32], and is designed to stress-test forward and inverse modelling tools in the presence of complex multiscale heterogeneity.

For the simulations considered in this work, we extract a target subregion of the full model, covering $20 \text{ km} \times 102 \text{ km} \times 28.3 \text{ km}$ (Figure 16). The material coefficients of our model for this test case are set to $a \equiv 1$ and $m(\mathbf{x}) = c^{-2}(\mathbf{x})$. The geometrical parameters are measured according to the minimal wavelength $\lambda_{\min} = 2\pi \min_{\mathbf{x}}(c(\mathbf{x}))/\omega$. The domain is discretised with an unstructured tetrahedral mesh, adapted to the local wavelength to ensure accurate resolution of the wavefield, with denser refinement near the bathymetry and across high-contrast interfaces.

For this simulation, we use an unstructured mesh that complies with the bathymetry. Below the bathymetry, the size of the elements is set according to the local wavelength such that we have approximately 4 points per wavelength for the reference angular frequency $\omega = 3.75\pi \text{ rad s}^{-1}$ (Figure 17).

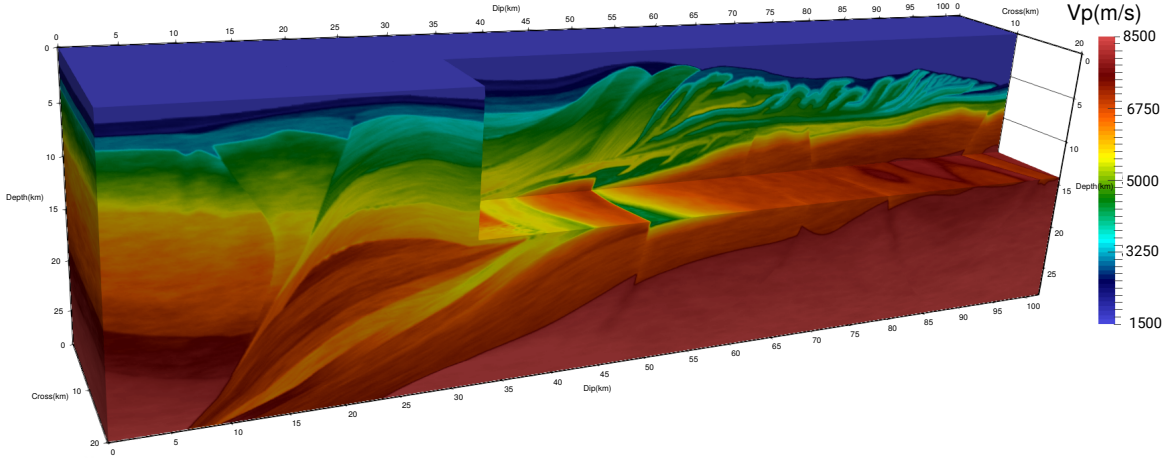


Figure 16: Target of the regional GO_3D_OBS model representing the crust of a subduction zone [31].

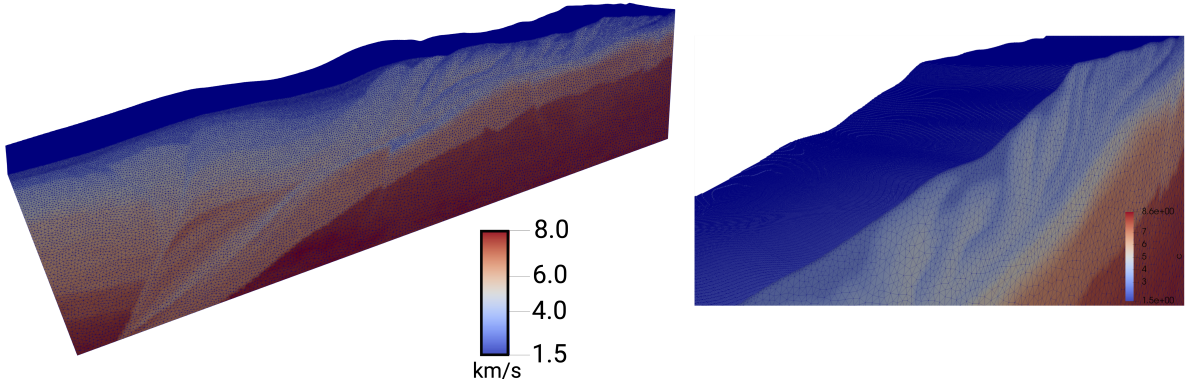


Figure 17: Tetrahedral mesh of the GO_3D_OBS model adapted to the local wavelength. Note that the mesh in the water layer is not shown in the Figure. Instead, the conformal meshing of the seabed is highlighted. The right panel shows a zoom.

Strong scaling test To further assess scalability in heterogeneous 3D media, we perform a *strong scaling test* on the crustal-geomodel benchmark. In this experiment, we consider two partitions with 1024 and 2048 subdomains.

The results are reported in Table 7 and we also report the number of GMRES iterations to reach the required tolerance as a function of the total coarse space size and choice of threshold parameter in Figure 18. The number of subdomains is provided in brackets in the legend entries.

L	$[\lambda_{\min}]$	N	n	H	$[\lambda_{\min}]$	n_s	$n_s^{\partial\Omega_s}$	1lvl	ext	harm	DtN	H_k						
								It	CS	CS	CS $_s$	It	CS	CS $_s$	It	CS	CS $_s$	
48.3	1024	22297073	4.8	35185	5416	380	122	204800	200	137	204800	200	>200	204800	200	>200	204800	200
48.3	2048	22297073	3.8	19864	3712	471	77	409600	200	102	409600	200	>200	409600	200	>200	409600	200

Table 7: Strong scaling experiment for the GO_3D_OBS test case.

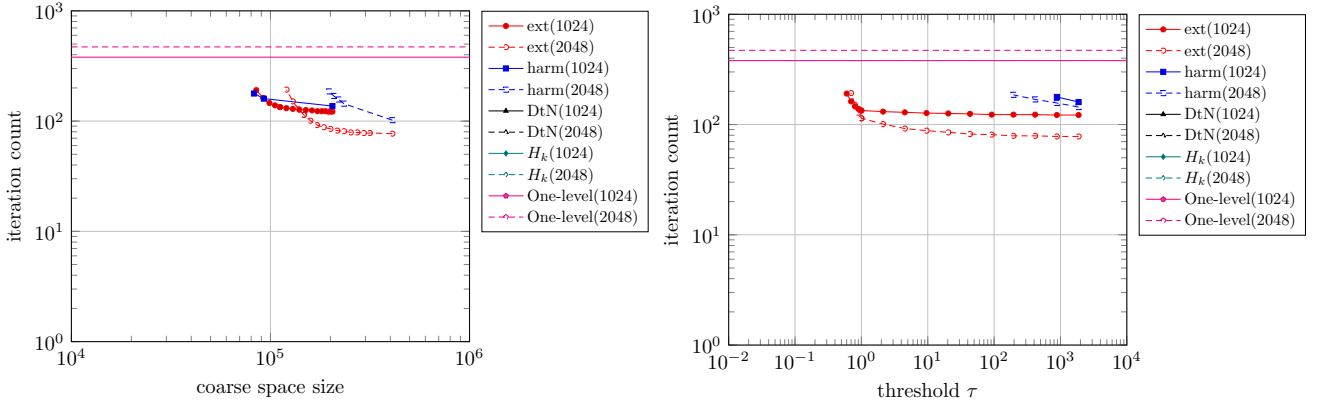


Figure 18: Influence of the coarse space size (left) and threshold choice (right) on the iteration count in a strong scaling experiment for the GO_3D_OBS test case.

Assessment and comparative conclusions for the crustal-geomodel test case

- Harmonic and extended-harmonic coarse spaces are able to provide a reduction in the iteration count compared to the one-level method. The smallest number of iterations is obtained for the extended-harmonic one, with more compact coarse spaces in the case with the largest number of subdomains.
- In contrast, both DtN and H_k -GenEO coarse spaces do not provide convergence for this challenging heterogeneous 3D test case.
- The harmonic coarse space required significantly larger values for the eigenvalue threshold parameter.

6 Conclusions

This study presents a comprehensive evaluation of spectral coarse spaces in two-level overlapping Schwarz methods for solving high-frequency Helmholtz problems in both homogeneous and heterogeneous media. The analysis spans a wide range of numerical settings, from idealised 2D test cases to large-scale 3D benchmarks such as the COBRA cavity and the GO_3D_OBS crustal geomodel.

A comparative overview of the key characteristics of each spectral coarse space is provided in Table 8. Our main findings can be summarised as follows:

- **Two-level domain decomposition is essential** for robust and scalable solvers at mid-to-high frequencies. All spectral coarse spaces studied outperform the one-level ORAS baseline by a wide margin.
- **Extended harmonic coarse spaces** offer the best trade-off between solver efficiency and coarse space size. They consistently deliver low GMRES iteration counts, even under weak scaling and in high-frequency 3D heterogeneous settings. We point out however that the eigenproblem is posed in an enlarged domain.
- **Harmonic coarse spaces** have a performance comparable to that of extended-harmonic coarse spaces. In some occurrences, in particular with a large number of subdomains, they require slightly larger coarse space sizes or a few more iterations compared to their extended counterpart.

- **DtN coarse spaces** are compact and competitive for moderate problem sizes but become less effective for larger domains and higher frequency, and breakdown can be observed in 3D. We remark a strong sensitivity with respect to the eigenvalue threshold parameter τ .
- **H_k -GenEO** exhibits strong robustness in 2D but incurs significantly higher computational cost due to larger coarse spaces, and breakdown can be observed in 3D. It remains an attractive choice when memory constraints are less critical.
- Additional implementation aspects—such as overlap width, partition of unity smoothness, and eigenvalue threshold tuning—affect performance and should be carefully optimised in practice.

Overall, the results validate the use of physics-informed spectral coarse spaces—especially harmonic and extended harmonic types—as effective strategies for achieving scalability and wavenumber robustness in Helmholtz solvers across a wide spectrum of applications.

A comparison of these domain decomposition preconditioners in terms of setup and GMRES run times in addition to iteration count and coarse space sizes has been left outside of the scope of this study but is of practical importance and could be a perspective for future work.

Problem	d	Medium	B.C.	Scaling	Extended	Harmonic	DtN	H_k -GenEO
Square	2D	homogeneous	Robin	strong	✓	✓	✓✓	✓
	2D	heterogeneous	Robin	strong	✓	✓	✓✓	✓
Medical imaging	2D	homogeneous	PML	strong	✓✓	✓✓	✓	✓
	2D	heterogeneous	PML	weak	✓✓	✓✓	✓	✓
Cobra cavity	3D	homogeneous	Robin	weak	✓✓	✓✓	✓/✗	✓/✗
Crustal geomodel	3D	heterogeneous	PML	strong	✓✓	✓✓	✗	✗

Table 8: An overview of which coarse spaces perform well in the different problem scenarios tests. A ✓ indicates that the method performs well, with ✓✓ indicating this method was most favourable in a particular instance. A ✗ indicates that a method provided relatively little to no gain over the one-level method.

References

- [1] H. Al Daas, P. Jolivet, F. Nataf, and P.-H. Tournier. *A Robust Two-Level Schwarz Preconditioner For Sparse Matrices*. 2024. arXiv: [2401.03915](https://arxiv.org/abs/2401.03915).
- [2] P. Amestoy, I. Duff, J.-Y. L’Excellent, and J. Koster. “A fully asynchronous multifrontal solver using distributed dynamic scheduling”. In: *SIAM J. Matrix Anal. Appl.* 23.1 (2001), pp. 15–41. URL: <http://mumps.enseeiht.fr>.
- [3] I. M. Babuska and S. A. Sauter. “Is the pollution effect of the FEM avoidable for the Helmholtz equation considering high wave numbers?” In: *SIAM J. Numer. Anal.* 34.6 (1997), pp. 2392–2423. DOI: [10.1137/S0036142993255035](https://doi.org/10.1137/S0036142993255035).
- [4] H. Beriot and A. Modave. “An automatic perfectly matched layer for acoustic finite element simulations in convex domains of general shape”. In: *International Journal for Numerical Methods in Engineering* 122 (2021), pp. 1239–1261. DOI: [10.1002/nme.6581](https://doi.org/10.1002/nme.6581).
- [5] A. Bermúdez, L. Hervella-Nieto, A. Prieto, and R. Rodríguez. “An exact bounded PML for the Helmholtz equation”. In: *C. R. Math. Acad. Sci. Paris* 339.11 (2004), pp. 803–808. DOI: [10.1016/j.crma.2004.10.006](https://doi.org/10.1016/j.crma.2004.10.006).
- [6] M. Bonazzoli, V. Dolean, I. G. Graham, E. A. Spence, and P.-H. Tournier. “Domain decomposition preconditioning for the high-frequency time-harmonic Maxwell equations with absorption”. In: *Math. Comp.* 88.320 (2019), pp. 2559–2604. DOI: [10.1090/mcom/3447](https://doi.org/10.1090/mcom/3447).
- [7] N. Bootland and V. Dolean. “On the Dirichlet-to-Neumann coarse space for solving the Helmholtz problem using domain decomposition”. In: *Numerical mathematics and advanced applications—ENUMATH 2019*. Vol. 139. Lect. Notes Comput. Sci. Eng. Springer, Cham, 2021, pp. 175–184. DOI: [10.1007/978-3-030-55874-1_16](https://doi.org/10.1007/978-3-030-55874-1_16).
- [8] N. Bootland and V. Dolean. “Can DtN and GenEO Coarse Spaces Be Sufficiently Robust for Heterogeneous Helmholtz Problems?” In: *Mathematical and Computational Applications* 27.3 (2022). DOI: [10.3390/mca27030035](https://doi.org/10.3390/mca27030035).
- [9] N. Bootland, V. Dolean, I. G. Graham, C. Ma, and R. Scheichl. “Overlapping Schwarz methods with GenEO coarse spaces for indefinite and nonself-adjoint problems”. In: *IMA J. Numer. Anal.* 43.4 (Aug. 2022), pp. 1899–1936. DOI: [10.1093/imanum/drac036](https://doi.org/10.1093/imanum/drac036).
- [10] N. Bootland, V. Dolean, I. G. Graham, C. Ma, and R. Scheichl. “GenEO coarse spaces for heterogeneous indefinite elliptic problems”. In: *Domain decomposition methods in science and engineering XXVI*. Vol. 145. Lect. Notes Comput. Sci. Eng. Springer, Cham, 2022, pp. 117–125. DOI: [10.1007/978-3-030-95025-5_10](https://doi.org/10.1007/978-3-030-95025-5_10).

- [11] N. Bootland, V. Dolean, P. Jolivet, and P.-H. Tournier. “A comparison of coarse spaces for Helmholtz problems in the high frequency regime”. In: *Comput. Math. Appl.* 98 (2021), pp. 239–253. DOI: [10.1016/j.camwa.2021.07.011](https://doi.org/10.1016/j.camwa.2021.07.011).
- [12] A. Brandt and I. Livshits. “Wave-ray multigrid method for standing wave equations”. In: *Electron. Trans. Numer. Anal.* 6 (1997), pp. 162–181.
- [13] T. Chaumont-Frelet, V. Dolean, M. Fry, I. G. Graham, and M. Langer. *Spectral coarse spaces based on indefinite operators: the H_k -GenEO method*. 2024. arXiv: [2406.06283](https://arxiv.org/abs/2406.06283).
- [14] L. Conen, V. Dolean, R. Krause, and F. Nataf. “A coarse space for heterogeneous Helmholtz problems based on the Dirichlet-to-Neumann operator”. In: *J. Comput. Appl. Math.* 271 (2014), pp. 83–99. DOI: [10.1016/j.cam.2014.03.031](https://doi.org/10.1016/j.cam.2014.03.031).
- [15] V. Dolean, P. Jolivet, P. Tournier, and S. Operto. “Large-scale frequency-domain seismic wave modeling on h-adaptive tetrahedral meshes with iterative solver and multi-level domain-decomposition preconditioners”. In: *90th Annual International Meeting, SEG Technical Program Expanded Abstracts 2020*. Society of Exploration Geophysicists, 2020, pp. 2683–2688. DOI: [10.1190/segam2020-3427414.1](https://doi.org/10.1190/segam2020-3427414.1).
- [16] V. Dolean, M. Fry, and M. Langer. *Improvements to the theoretical estimates of the Schwarz preconditioner with Δ -GenEO coarse space for the indefinite Helmholtz problem*. 2024. arXiv: [2403.18378](https://arxiv.org/abs/2403.18378).
- [17] V. Dolean, M. J. Gander, S. Lanteri, J.-F. Lee, and Z. Peng. “Effective transmission conditions for domain decomposition methods applied to the time-harmonic curl-curl Maxwell’s equations”. In: *J. Comput. Phys.* 280 (2015), pp. 232–247. DOI: [10.1016/j.jcp.2014.09.024](https://doi.org/10.1016/j.jcp.2014.09.024).
- [18] V. Dolean, P. Jolivet, and F. Nataf. *An introduction to domain decomposition methods*. Society for Industrial and Applied Mathematics (SIAM), Philadelphia, PA, 2015, pp. x+238. DOI: [10.1137/1.9781611974065.ch1](https://doi.org/10.1137/1.9781611974065.ch1).
- [19] V. Dolean, P. Jolivet, P. Tournier, and S. Operto. “Iterative frequency-domain seismic wave solvers based on multi-level domain-decomposition preconditioners”. In: *EAGE 2020 Annual Conference & Exhibition Online*. 1. European Association of Geoscientists & Engineers. 2020, pp. 1–5.
- [20] V. Dolean, F. Nataf, R. Scheichl, and N. Spillane. “Analysis of a two-level Schwarz method with coarse spaces based on local Dirichlet-to-Neumann maps”. In: *Comput. Methods Appl. Math.* 12.4 (2012), pp. 391–414. DOI: [10.2478/cmam-2012-0027](https://doi.org/10.2478/cmam-2012-0027).
- [21] O. G. Ernst and M. J. Gander. “Why it is difficult to solve Helmholtz problems with classical iterative methods”. In: *Numerical analysis of multiscale problems*. Vol. 83. Lect. Notes Comput. Sci. Eng. Springer, Heidelberg, 2012, pp. 325–363. DOI: [10.1007/978-3-642-22061-6_10](https://doi.org/10.1007/978-3-642-22061-6_10).
- [22] C. Farhat, P. Avery, R. Tezaur, and J. Li. “FETI-DPH: a dual-primal domain decomposition method for acoustic scattering”. In: *J. Comput. Acoust.* 13.3 (2005), pp. 499–524. DOI: [10.1142/S0218396X05002761](https://doi.org/10.1142/S0218396X05002761).
- [23] C. Farhat, A. Macedo, and M. Lesoinne. “A two-level domain decomposition method for the iterative solution of high frequency exterior Helmholtz problems”. In: *Numer. Math.* 85.2 (2000), pp. 283–308. DOI: [10.1007/PL00005389](https://doi.org/10.1007/PL00005389).
- [24] J. Fish and Y. Qu. “Global-basis two-level method for indefinite systems. I. Convergence studies”. In: *Internat. J. Numer. Methods Engrg.* 49.3 (2000), pp. 439–460. DOI: [10.1002/1097-0207\(20000930\)49:3<439::AID-NME981>3.0.CO;2-A](https://doi.org/10.1002/1097-0207(20000930)49:3<439::AID-NME981>3.0.CO;2-A).
- [25] J. Galkowski, D. Lafontaine, E. A. Spence, and J. Wunsch. “The hp -FEM applied to the Helmholtz equation with PML truncation does not suffer from the pollution effect”. In: *Commun. Math. Sci.* 22.7 (2024), pp. 1761–1816. DOI: [10.4310/cms.240918021620](https://doi.org/10.4310/cms.240918021620).
- [26] J. Galkowski and E. A. Spence. *Convergence theory for two-level hybrid Schwarz preconditioners for high-frequency Helmholtz problems*. 2025. arXiv: [2501.11060](https://arxiv.org/abs/2501.11060).
- [27] M. J. Gander and H. Zhang. “A class of iterative solvers for the Helmholtz equation: factorizations, sweeping preconditioners, source transfer, single layer potentials, polarized traces, and optimized Schwarz methods”. In: *SIAM Rev.* 61.1 (2019), pp. 3–76. DOI: [10.1137/16M109781X](https://doi.org/10.1137/16M109781X).
- [28] J. Garnier, L. Giovangigli, Q. Goepfert, and P. Millien. *Scattered wavefield in the stochastic homogenization regime*. 2023. arXiv: [2309.07777](https://arxiv.org/abs/2309.07777).
- [29] J. Garnier, L. Giovangigli, Q. Goepfert, and P. Millien. *Probing the speckle to estimate the effective speed of sound, a first step towards quantitative ultrasound imaging*. 2025. arXiv: [2505.07566](https://arxiv.org/abs/2505.07566).
- [30] S. Gong, I. G. Graham, and E. A. Spence. “Domain decomposition preconditioners for high-order discretizations of the heterogeneous Helmholtz equation”. In: *IMA J. Numer. Anal.* 41.3 (2021), pp. 2139–2185. DOI: [10.1093/imanum/draa080](https://doi.org/10.1093/imanum/draa080).
- [31] A. Górszczyk and S. Operto. “GO_3D_OBS: the multi-parameter benchmark geomodel for seismic imaging method assessment and next-generation 3D survey design (version 1.0)”. In: *Geoscientific Model Development* 14.3 (2021), pp. 1773–1799.

- [32] A. Górszczyk, S. Operto, and M. Malinowski. “Toward a robust workflow for deep crustal imaging by FWI of OBS data: the eastern Nankai Trough revisited”. In: *Journal of Geophysical Research: Solid Earth* 122.6 (2017), pp. 4601–4630.
- [33] I. G. Graham, E. A. Spence, and E. Vainikko. “Recent Results on Domain Decomposition Preconditioning for the High-Frequency Helmholtz Equation Using Absorption”. In: *Lahaye D., Tang J., Vuik K. (eds) Modern Solvers for Helmholtz Problems. Geosystems Mathematics. Birkhäuser, Cham* (2017). DOI: [10.1007/978-3-319-28832-1_1](https://doi.org/10.1007/978-3-319-28832-1_1).
- [34] I. G. Graham, E. A. Spence, and J. Zou. “Domain decomposition with local impedance conditions for the Helmholtz equation with absorption”. In: *SIAM J. Numer. Anal.* 58.5 (2020), pp. 2515–2543. DOI: [10.1137/19M1272512](https://doi.org/10.1137/19M1272512).
- [35] R. Haferssas, P. Jolivet, and F. Nataf. “An additive Schwarz method type theory for Lions’s algorithm and a symmetrized optimized restricted additive Schwarz method”. In: *SIAM J. Sci. Comput.* 39.4 (2017), A1345–A1365. DOI: [10.1137/16M1060066](https://doi.org/10.1137/16M1060066).
- [36] I. Harari, M. Slavutin, and E. Turkel. “Analytical and numerical studies of a finite element PML for the Helmholtz equation”. In: *J. Comput. Acoust.* 8 (2000), pp. 121–137. DOI: [10.1142/S0218396X00000096](https://doi.org/10.1142/S0218396X00000096).
- [37] V. Hernandez, J. E. Roman, and V. Vidal. “SLEPc: A scalable and flexible toolkit for the solution of eigenvalue problems”. In: *ACM Transactions on Mathematical Software* 31.3 (2005), pp. 351–362. URL: <https://slepc.upv.es>.
- [38] Q. Hu and Z. Li. *A novel coarse space applying to the weighted Schwarz method for Helmholtz equations*. 2024. arXiv: [2402.06905](https://arxiv.org/abs/2402.06905).
- [39] J.-M. Jin. *The Finite Element Method in Electromagnetics*. John Wiley & Sons, 2015.
- [40] G. Karypis and V. Kumar. *A software package for partitioning unstructured graphs, partitioning meshes, and computing fill-reducing orderings of sparse matrices*. Tech. rep. University of Minnesota, Department of Computer Science and Engineering, Army HPC Research Center, Minneapolis, MN, 1998.
- [41] J. Liu and J.-M. Jin. “Scattering analysis of a large body with deep cavities”. In: *IEEE Transactions on Antennas and Propagation* 51.6 (2003), pp. 1157–1167. DOI: [10.1109/TAP.2003.812280](https://doi.org/10.1109/TAP.2003.812280).
- [42] C. Ma, C. Alber, and R. Scheichl. *Two-level restricted additive Schwarz preconditioner based on multiscale spectral generalized FEM for heterogeneous Helmholtz problems*. 2024. arXiv: [2409.06533](https://arxiv.org/abs/2409.06533).
- [43] F. Nataf and E. Parolin. *Coarse spaces for non-symmetric two-level preconditioners based on local generalized eigenproblems*. 2024. arXiv: [2404.02758](https://arxiv.org/abs/2404.02758).
- [44] F. Nataf, H. Xiang, V. Dolean, and N. Spillane. “A coarse space construction based on local Dirichlet-to-Neumann maps”. In: *SIAM J. Sci. Comput.* 33.4 (2011), pp. 1623–1642. DOI: [10.1137/100796376](https://doi.org/10.1137/100796376).
- [45] S. Operto, P. Amestoy, H. Aghamiry, S. Beller, A. Buttari, et al. “Is 3D frequency-domain FWI of full-azimuth/long-offset OBN data feasible? The Gorgon data FWI case study”. In: *The Leading Edge* 42.3 (2023), pp. 173–183.
- [46] N. Spillane, V. Dolean, P. Hauret, F. Nataf, C. Pechstein, et al. “Abstract robust coarse spaces for systems of PDEs via generalized eigenproblems in the overlaps”. In: *Numer. Math.* 126.4 (2014), pp. 741–770. DOI: [10.1007/s00211-013-0576-y](https://doi.org/10.1007/s00211-013-0576-y).
- [47] P.-H. Tournier, P. Jolivet, V. Dolean, H. S. Aghamiry, S. Operto, et al. “3D finite-difference and finite-element frequency-domain wave simulation with multilevel optimized additive Schwarz domain-decomposition preconditioner: a tool for full-waveform inversion of sparse node data sets”. In: *GEOPHYSICS* 87.5 (2022), T381–T402. DOI: [10.1190/geo2021-0702.1](https://doi.org/10.1190/geo2021-0702.1).
- [48] P.-H. Tournier, P. Jolivet, and F. Nataf. *FFDDM: FreeFem Domain Decomposition Method*. 2019. URL: <https://doc.freefem.org/documentation/ffddm/index.html>.
- [49] A. Zarmi and E. Turkel. “A general approach for high order absorbing boundary conditions for the Helmholtz equation”. In: *J. Comput. Phys.* 242 (2013), pp. 387–404. DOI: [10.1016/j.jcp.2013.02.042](https://doi.org/10.1016/j.jcp.2013.02.042).